







FAST Observations of the Microstructure in Interpulse Pulsars*

WEI LI ^{1,2,3} SHIJUN DANG ^{1,4} NA WANG ^{2,3} CHENGMIN ZHANG,⁵ JINGBO WANG,⁶ JIANPING YUAN ² FEIFEI KOU,²
YANQING CAI ^{1,3,5} ZURONG ZHOU,^{7,8} SHUANGQIANG WANG,² LUNHUA SHANG,^{1,4} JUNTAO BAI,² YIRONG WEN ^{2,3,6}
JING ZOU,^{2,3,6} ZHIXIANG YU,^{1,4}
(AAS JOURNALS DATA EDITORS)

¹*School of Physics and Electronic Science, Guizhou Normal University, Guiyang 550001, China*

²*Xinjiang Astronomical Observatory, Chinese Academy of Sciences, Urumqi, Xinjiang 830011, China*

³*University of Chinese Academy of Sciences, Beijing 100049, China*

⁴*Guizhou Provincial Key Laboratory of Radio Astronomy and Data Processing, Guizhou Normal University, Guiyang 550001, China*

⁵*National Astronomical Observatories, Chinese Academy of Sciences, Beijing 100101, China*

⁶*Institute of Optoelectronic Technology, Lishui University, Lishui, Zhejiang 323000, China*

⁷*National Time Service Center, Chinese Academy of Sciences, Xi'an 710600, China*

⁸*Key Laboratory of Time Reference and Applications, Chinese Academy of Sciences, Xi'an 710600, China*

ABSTRACT

In this study, we investigate the microstructure properties of four pulsars (PSRs J0953+0755 (B0950+08), J0627+0706, J0826+2637 (B0823+26) and J1946+1805 (B1944+17)) using the Five-hundred-meter Aperture Spherical radio Telescope (FAST), with particular emphasis on identifying microstructure within interpulse (IP). Through the application of autocorrelation function (ACF) analysis and fast Fourier transform (FFT) techniques, we have systematically examined the periodicity of microstructure in these pulsars. Our findings represent the first successful detection of microstructure within IP. Furthermore, we conducted a comprehensive statistical analysis comparing the characteristic timescales (τ_μ) and the characteristic periods P_μ of quasi-periodic microstructure between the main pulse (MP) and IP, and our results indicate that the τ_μ and P_μ of microstructure across components appear consistent within measurement errors for PSR J0627+0706, but microstructure in IP are relatively smaller than those in MP for PSR J0953+0755. Furthermore, the relationship between P_μ of microstructure and the rotation period in neutron star populations was reconfirmed: $P_\mu(\text{ms}) = (1.337 \pm 0.114) \times P(\text{s})^{(1.063 \pm 0.038)}$.

Keywords: Pulsars (1306) — Radio Pulsars (1353)

1. INTRODUCTION

Pulsars are rapidly rotating neutron stars characterized by intense magnetic fields. Their pulse emissions exhibit significant variations from one period to another. Numerous intriguing single-pulse behaviors have been identified in pulsars, including mode changing, subpulse drifting, and nulling (Wang et al. 2007), among others. Investigating these single-pulse phenomena provides valuable insights into the magnetospheric structure and radiation mechanisms of pulsars.

dangsj@gznu.edu.cn (S.J. Dang)

na.wang@xao.ac.cn (N. Wang)

1983wangjingbo@163.com (J.B. Wang)

* Released on May, 2, 2025

Microstructure, which manifests as rapid intensity fluctuations within single-pulses on submillisecond timescales, represents another fascinating single-pulse phenomenon. Shortly after the initial discovery of pulsars, [Craft et al. \(1968a\)](#) made the first observations of the microstructure in these celestial objects. Subsequent research has led to the detection of microstructure in an increasing number of pulsars, revealing their intriguing properties. In particular, microstructure has also been observed in the Crab pulsar ([Hankins et al. 2003](#); [Jessner et al. 2010](#)) and the Vela pulsar ([Johnston et al. 2001](#); [Kramer et al. 2002](#)), offering further opportunities to improve our understanding of these two prominent pulsars.

There is increasing evidence shows that certain microstructure exhibits quasiperiodic behavior ([Boriakoff 1976](#); [Ferguson et al. 1976](#); [Cordes 1976](#); [Cordes & Hankins 1977](#); [Boriakoff & Ferguson 1981](#); [Soglasnov et al. 1981](#)). [Hankins \(1971a\)](#) first observed microstructure in PSR B0950+08 with τ_μ shorter than $10\mu\text{s}$, and identified quasi-periodic microstructure with P_μ ranging from 300 to $700\mu\text{s}$. Subsequently, [Cordes et al. \(1990\)](#) detected quasi-periodic microstructure in several pulsars, including PSRs B0950+08, B1133+16, B0809+74, B1944+17 and B2016+28. Notably, quasi-periodic microstructure was also detected in a ultra-long-period pulsar J0901–4046 with a rotation period of approximately 76 s ([Caleb et al. 2022a](#)) and a 6.45-h-period coherent radio transient ASKAP J183950.5–075635.0 ([Lee et al. 2025](#)).

Interestingly, observational studies have revealed a potential connection between microstructure properties and the rotation period (P) of pulsars. [Cordes \(1976\)](#) established a relationship between the τ_μ range of microstructure ($\Delta\tau_\mu$) and the pulsar’s rotation period: $\Delta\tau_\mu \approx 10^{-3}P$. Furthermore, [Kramer et al. \(2002\)](#) derived a relationship between τ_μ and P : $\tau_\mu(\mu\text{s}) = (600 \pm 100)P(\text{s})^{1.1 \pm 0.2}$, emphasizing that this linear dependence is not an artifact of the time resolution of observational instruments. [Mitra et al. \(2015\)](#) (hereafter M15) further demonstrated that P_μ tends to increase with the pulsar’s rotation period, although no clear correlation was found between P_μ and other pulsar parameters, such as the period derivative, characteristic age, or surface magnetic field.

Efforts have also been made to detect microstructure in millisecond pulsars (MSPs), which require exceptionally high time resolution. If the empirical relationship between τ_μ and P for normal-period pulsars ([Cordes 1976](#)) is extended to MSPs, the τ_μ range of their microstructure would be less than 30 ns for MSPs with rotation periods below 30 ms (if we only divide the pulse into 1024 phase bins). This implies that observations must achieve a time resolution of at least 30 ns to resolve the fine microstructure in MSPs. At a time resolution of $80\mu\text{s}$, [Jenet et al. \(1998\)](#) found no evidence of microstructure in MSP J0437–4715. Similarly, [Liu et al. \(2016\)](#) reported no detection of microstructure in MSP 1713+0747 at a resolution of 140 ns. Finally, [De et al. \(2016\)](#) made the first successful detection of microstructure in MSPs J0437–4715 and J2145–0750 at resolutions of $0.384\mu\text{s}$ and $0.96\mu\text{s}$, respectively. They found that the properties of microstructure in MSPs are analogous to those in normal-period pulsars, including quasi-periodic behavior. Furthermore, they established a relationship between P_μ and the rotation periods of MSPs: $P_\mu(\mu\text{s}) = 1.06 \pm 0.63P(\text{ms})^{0.96 \pm 0.09}$, which aligns with the relationship observed in normal-period pulsars. Subsequently, [Liu et al. \(2022\)](#) also identified microstructure in MSPs J1022+1001, J2145–0750, and J1744–1134, demonstrating that the relationship between P_μ and P they derived is consistent with the earlier findings of [De et al. \(2016\)](#). Currently, studies on the microstructure of MSPs remain limited. Further observational research on microstructure in MSPs may enhance our understanding of the similarities and differences in the radiation mechanisms between MSPs and normal-period pulsars.

Here, we pose a thought-provoking question: is microstructure unique to radio pulsars, or does it also manifest in other radio sources? Evidence suggests that microstructure-like phenomena indeed exist in other radio sources. For instance, [Caleb et al. \(2022b\)](#) observed microstructure in the radio magnetar XTE J1810–197. Similarly, [Majid et al. \(2021\)](#) identified a quasi-periodic structure with a period of approximately $2.3\mu\text{s}$ in the Fast Radio Burst (FRB) 20200120E. Quasi-periodic structure was also detected in FRBs 20201020A ([Pastor-Marazuela et al. 2023](#)), 20201124A ([Niu et al. 2022](#)), 20191221A, 20210206A and 20210213A ([Chime/Frb Collaboration et al. 2022](#)). Furthermore, quasi-periodic microstructure was also observed in Rotating Radio Transients (RRATs) using the FAST, including RRATs J1918–0449 ([Chen et al. 2022](#)), J0139+3336 ([Dang et al. 2024](#)), and J1913+1330 ([Zhang et al. 2024](#); [Zhong et al. 2024](#); [Tang et al. 2025](#)). These observations intriguingly suggest a connection between pulsars, magnetars, RRATs, and FRBs through the common feature of quasi-periodic microstructure-like phenomena. Even more compelling, [Kramer et al. \(2024\)](#) derived two key relationships among diverse radio sources: (1) the linear relationship between the rotation periods and the τ_μ of quasi-periodic substructure: $P_\mu(\text{ms}) = (0.59 \pm 0.03) \times P(\text{s})^{(0.99 \pm 0.02)}$, and (2) the linear relationship between the rotation periods and the characteristic periods: $\tau_\mu(\text{ms}) = (0.94 \pm 0.04) \times P(\text{s})^{(0.97 \pm 0.05)}$. These relationships imply that the radiation mechanisms of these distinct radio sources may share underlying similarities.

Table 1. Observation Information of Four Interpulse Pulsars

JName	P (ms)	τ_c (Myr)	Obs Time (yyyy/mm/dd)	N	Time Resolution (μ s)	N_{bin}
J0627+0706	0.475884937713(3)	0.253	2019/11/26	1257	49.152	4096
J0826+2637	0.53066051169(3)	4.92	2019/11/26	701	98.304	8192
J0953+0755	0.2530651649482(9)	17.5	2018/07/18	4678	49.152	4096
J1946+1805	0.4406184769108(8)	290	2019/12/04	1327	98.304	4096

NOTE—Columns 1–3 list the pulsar names, rotation periods, and characteristic ages, respectively, while columns 4–7 provide the observation time, the number of single pulses, the time resolution of observation, and the phase bins of the single pulses.

Consequently, in-depth studies of microstructure may be crucial for advancing our understanding of neutron star populations and even the origins and radiation mechanisms of FRBs.

Inter-pulse pulsars represent a unique subclass of pulsars characterized by emission profiles consisting of both a MP and an IP. The canonical lighthouse model of pulsars naturally predicts the occurrence of IP. According to this model, two emission beams are aligned along the open field lines of a dipolar magnetic field. Specifically, when the inclination angle α approaches 90 degrees (indicating an almost orthogonal rotation), observers can detect emission from both beams associated with two diametrically opposite magnetic poles. This configuration is known as the double-pole IP model. In this scenario, the two pulse components are separated by approximately 180 degrees in longitude, with no detectable low-level emission between the MP and IP. The duty cycles of each component are relatively short, typically accounting for only a few percent of the pulsar’s period. An alternative explanation for IP generation is provided by the single-pole model (Manchester & Lyne 1977). This model assumes a small angle of inclination α , which corresponds to a nearly aligned rotation. In this case, the pulse widths are significantly broader than those in the double-pole IP model, often spanning the entire or most of the pulsar period. Even when the two components are separated, a low-intensity emission bridge is typically observed between them (Maciesiak et al. 2011).

In this study, we aim to detect and analyze the microstructure in both MP and IP of pulsars, with the goal of exploring the similarities and differences between microstructure in these two components. Such investigations may provide valuable insights into the radiation mechanisms of MP and IP. Using high-quality data from the FAST, we conduct a detailed analysis of the microstructure in four interpulse pulsars. The structure of this paper is organized as follows: Section 2 describes the observational setup, data processing procedures. Section 3 provides the analysis methods. The results of our study are presented in Section 4, while Sections 5 and 6 offer a detailed discussion and a concise summary of our findings, respectively.

2. OBSERVATION AND DATA PROCESS

We acquired single-pulse data for interpulse pulsars from the publicly accessible FAST database. The observations were conducted using the L-band receiver of FAST, which covers a frequency range of 1050 MHz to 1450 MHz. Detailed information regarding the pulsars in our sample and the observational parameters are summarized in Table 1.

The data processing involved the following steps. First, we applied the timing ephemeris from the ATNF pulsar catalog (PSRCAT-V2.1.1)¹ (Manchester et al. 2005). Subsequently, we folded the data using the DSPSR² package (van Straten & Bailes 2011) to produce single-pulse stacks with distinct phase bins per period for each pulsar. The phase bin details are provided in Table 1. Finally, we used the PAZ and PAZI plugins in the PSRCHIVE³ software to mitigate radio frequency interference (RFI) (Hotan et al. 2004). We first deleted data affected by narrow-band and impulsive RFI and 5% of the band edges using PAZ plugin. Then we used PAZI plugin to check the pulse profiles and deleted frequency channels affected by RFI.

3. METHODS

After completing the data processing, we conducted an analysis of the microstructure in both the MP and IP. For determining the τ_μ and P_μ of the microstructure, we primarily followed the method outlined in M15, albeit with some modifications. The key steps are as follows:

¹ <https://www.atnf.csiro.au/people/pulsar/psrcat/>

² <https://dspsr.sourceforge.net/>

³ <https://psrchive.sourceforge.net/>

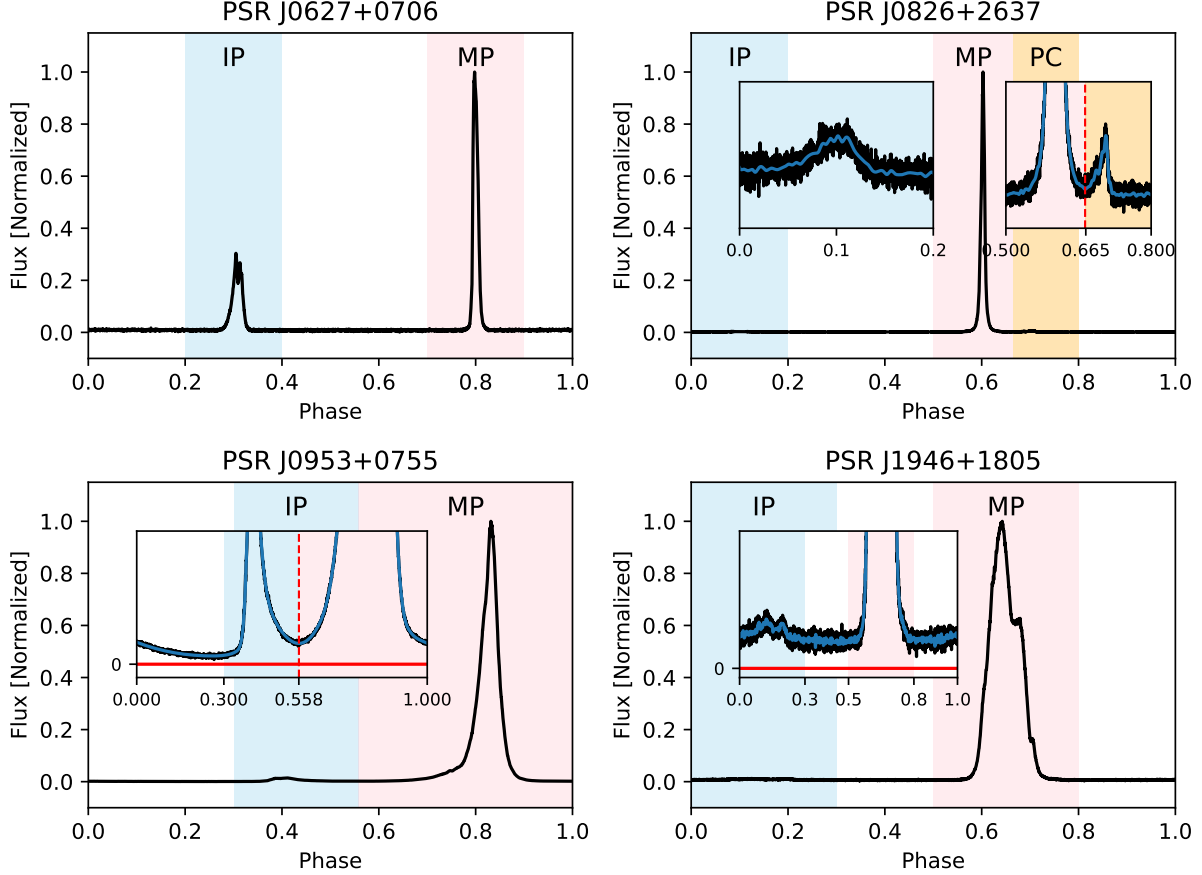


Figure 1. The profiles of Pulsars. Each of the four panels illustrates the normalized integrated profile of a pulsar, including an inset that zooms in on the pulse at a specific phase range. The MP, IP, and PC components are annotated with pink, blue, and orange rectangles, respectively. Denoised profiles are represented by the blue lines. Vertical red lines in the insets of the top-right and bottom-left panels mark the divisions between adjacent components.

Table 2. Delineation of Components in Pulsars

JName	IP	MP	PC
J0627+0706	0.2–0.4	0.7–0.9	—
J0826+2637	0–0.2	0.5–0.665	0.665–0.8
J0953+0755	0.3–0.558	0.558–1	—
J1946+1805	0–0.3	0.5–0.8	—

NOTE—Column 1 displays the pulsar names, and Columns 2 through 4 indicate the phase ranges of the IP, MP, and PC components, respectively.

- 1. Defining pulse components** Prior to analyzing the microstructure within the profile components, we first established a reasonable delineation of these components, as illustrated in Figure 1 and Table 2. Since the profile components of PSRs J0627+0706 and J1946+1805 are distinctly separated, we were able to visually estimate the component boundaries. For PSR J0826+2637, the IP component is easily distinguishable, but the MP and post-cursor (PC) components are closely spaced. We reduced noise by applying a low-pass filter to the profile and identified the boundary between the two components as the phase of minimum intensity. This method was also used to separate the MP and IP components of PSR J0953+0755. While our delineation approach is not

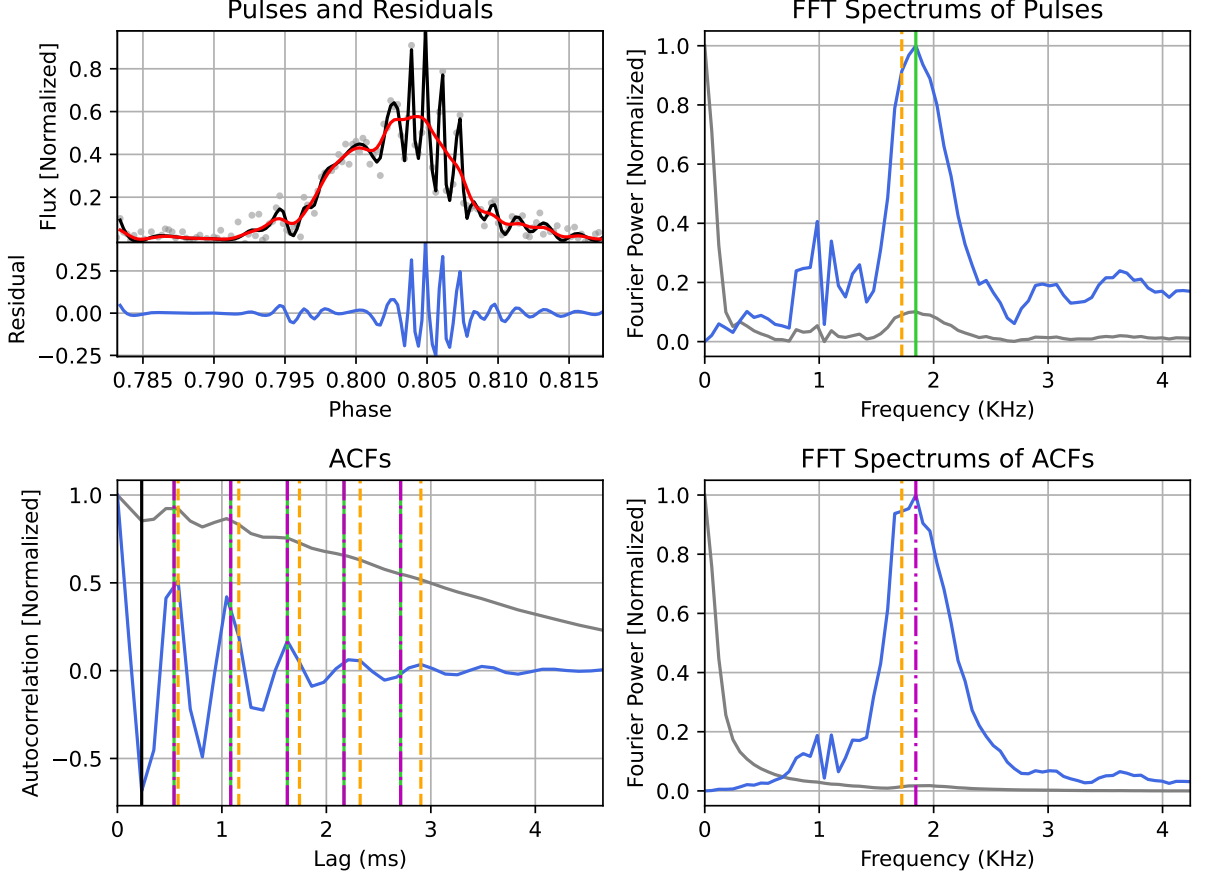


Figure 2. Pulse 136: A representative example of quasi-periodic microstructure in MP of PSR J0627+0706. Top-left panel: The gray dots represent the original pulse profile, while the black line shows the denoised pulse. The red line corresponds to smoothed pulses obtained using smoothing bandwidths of $0.075 \times N_{on}$. The residual of the smoothed pulse is plotted at the bottom. Lower-left panel: The blue line depict the normalized ACFs of the pulse residual. The solid black vertical line indicate the τ_μ of the microstructure. The orange dashed vertical lines represent values of one to five times the P_μ of the quasi-periodic microstructure derived from the first method; the green solid vertical lines show values of one to five times P_μ obtained from the FFT of the pulse residual, and the magenta dashdot vertical lines correspond to values of one to five times P_μ calculated from the FFT of the ACF of the pulse residual.

Upper-right panel: The normalized FFT spectra of the denoised pulse and its residual. Lower-right panel: The normalized FFT spectra of the ACF of the denoised pulse and its residual.

based on a rigorous definition, the subsequent findings confirm that it is entirely adequate for investigating the microstructure across different components.

2. **Data screening:** To more precisely analyze the microstructure, we select pulses with a signal-to-noise ratio (SNR) greater than 15, where the SNR is defined as the ratio of the peak value within the on-pulse region to the root mean square (RMS) of the off-pulse region. Additionally, we require that at least five phase points within the on-pulse region exceed three times the standard deviation of the off-pulse region.
3. **Noise processing:** We employed smoothing spline regression, a non-parametric regression method, to separate potential signals from noise for each single pulse. This approach makes only assumptions about a true but unknown regression function without specifying its mathematical form in advance (see M15 for a detailed description of this method). Our results indicate that this method effectively removes noise while maintaining the intrinsic structure of the pulses, as illustrated in the top-left panels of Figures 2 and 3. In these figures, the gray dots represent the original pulse profiles, while the black lines depict the denoised pulses.

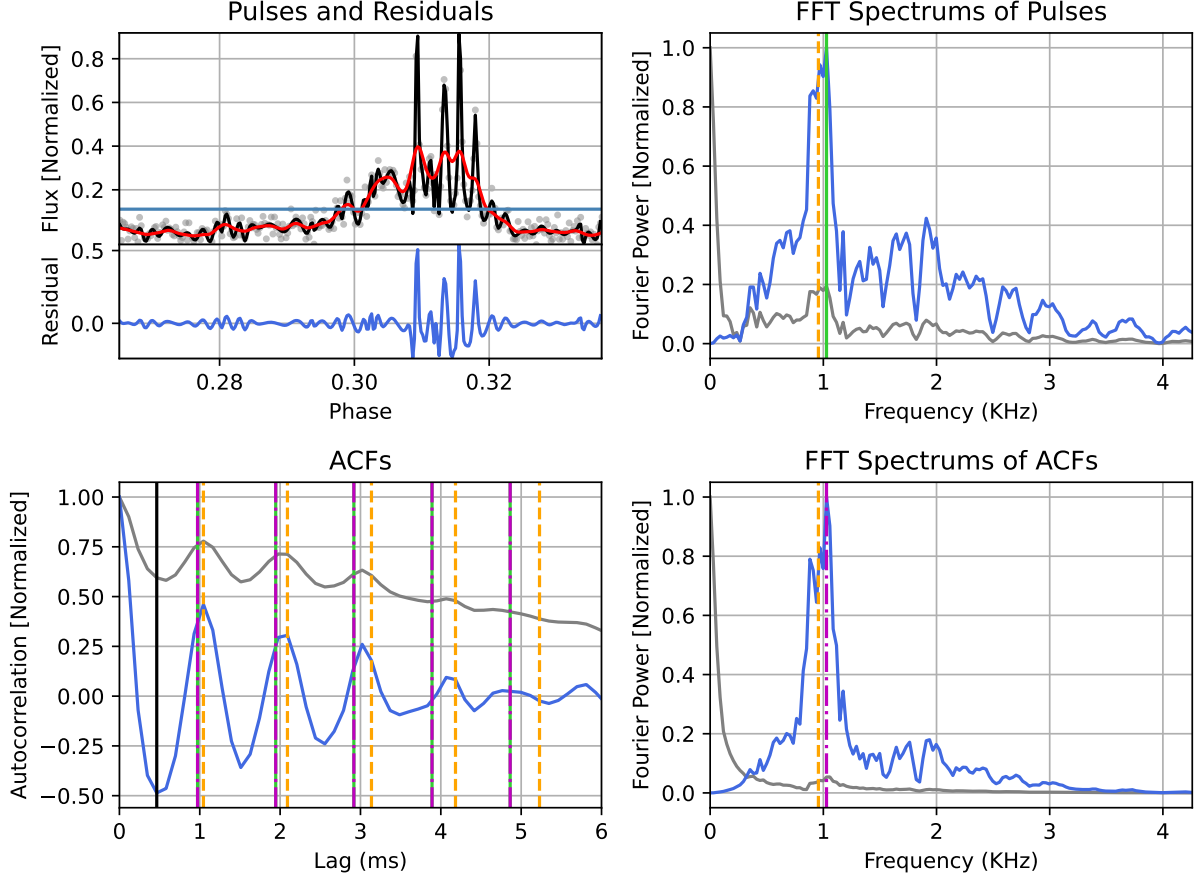


Figure 3. Pulse 212: A representative example of quasi-periodic microstructure observed in the IP of PSR J0627+0706. The light blue horizontal solid line in the top-left panel represent three times the standard deviation of the off-pulse region. All other features and annotations follow the same conventions as described in Figure 2.

4. **Removing low-frequency power and obtaining pulse residuals:** After completing the above steps, we initially attempted to calculate the ACF of the pulse directly to determine the τ_μ of the microstructure and the P_μ of the quasi-periodic microstructure. However, this approach presents a challenge: the ACF of the pulse may be dominated by low-frequency power. To mitigate this issue and better reveal the periodicity of the microstructure, we aimed to remove the strong low-frequency components from the single pulse. Following the method in M15, we applied the Nadaraya-Watson kernel method to smooth the pulses (see M15 for details).

For the selection of the smoothing bandwidth H , which controls the degree of smoothness, we adopted a strategy similar to but not identical to that of M15. M15 noted that $H > 0.1 \times N_{on}$ resulted in overly smoothed pulses, while $H < 0.05 \times N_{on}$ caused the smoothed pulses to closely follow the denoised pulses. Due to the lack of a definitive criterion for selecting the optimal smoothing bandwidth, M15 used three distinct bandwidths H ($0.05 \times N_{on}$, $0.075 \times N_{on}$ and $0.1 \times N_{on}$) and analyzed the microstructure separately for each. Here, N_{on} represents the number of phase bins of the on-pulse phase range of a single pulse.

In practice, we observed that the differences in results caused by varying smoothing bandwidths within the range of $0.05 \times N_{on}$ and $0.1 \times N_{on}$ are not significant, at least within the error margins displayed in M15. Therefore, we have directly chosen a smoothing bandwidth of $0.075 \times N_{on}$ for the smoothing process. After smoothing the denoised pulse, we derived the pulse residuals by subtracting the smoothed pulses from the denoised pulse (see the top-left panel in Figure 2).

Table 3. Microstructure Information of Four Interpulse Pulsars

JName	Component	N	N_h	N_m	τ_μ (ms)	P_μ (ms)
J0627+0706	MP	1257	1243	454	$0.46^{+0.00}_{-0.23}$	$0.82^{+0.17}_{-0.12}$
J0627+0706	IP	1257	792	42	$0.46^{+0.00}_{-0.11}$	$0.94^{+0.22}_{-0.24}$
J0826+2637	MP	701	648	303	$0.26^{+0.06}_{-0.07}$	$0.49^{+0.13}_{-0.10}$
J0826+2637	PC	701	9	7	$0.26^{+0.06*}_{-0.00}$	$0.54^{+0.02*}_{-0.05}$
J0953+0755	MP	4678	4651	2334	$0.25^{+0.06}_{-0.00}$	$0.50^{+0.15}_{-0.10}$
J0953+0755	IP	4678	1021	381	$0.19^{+0.06}_{-0.00}$	$0.38^{+0.11}_{-0.07}$
J1946+1805	MP	1327	454	95	$0.43^{+0.00}_{-0.11}$	$0.75^{+0.16}_{-0.16}$

NOTE—Columns 1 and 2 list the pulsar names and the components of pulses, respectively. Columns 3, 4 and 5 provide the total number of pulses, the number of high signal-to-noise ratio pulses (N_h) and the number of pulses with quasi-periodic microstructure (N_m). Columns 6 and 7 present the τ_μ and the P_μ of quasi-periodic microstructure. Additionally, data points marked with a superscript * indicate results that lack statistical significance.

5. **Calculating ACFs:** We computed the ACFs of the pulse residuals. To facilitate a comparison between different ACFs, we also calculated the ACF of the denoised pulse and normalized all ACFs (see the lower-left panel in Figure 2).
6. **Determine τ_μ of microstructure:** We selected the time delay corresponding to the first minimum of the ACF as the τ_μ of the microstructure.
7. **Determine P_μ of microstructure:** Determining the P_μ of quasi-periodic microstructure is more challenging compared to determining the τ_μ . We employed three methods to determine P_μ :
 - (1) We selected the time delay corresponding to the first minimum of the ACF as the P_μ of the microstructure.
 - (2) We performed a FFT on the pulse residual and used the reciprocal of the frequency corresponding to the peak in the FFT spectrum as a candidate value for P_μ .
 - (3) We performed a FFT on the ACF of the pulse residual and used the reciprocal of the frequency corresponding to the peak in the FFT spectrum as P_μ of the pulse.

As illustrated in the lower-left panel of Figure 2, the orange dashed vertical lines represent values of one to five times the P_μ of the quasi-periodic microstructure derived from the first method; the green solid vertical lines show values of one to five times P_μ obtained from the FFT of the pulse residual, and the magenta dashdot vertical lines correspond to values of one to five times P_μ calculated from the FFT of the ACF of the pulse residual. It should be noted that if the P_μ obtained by different methods are not significantly different, these lines will appear visually overlapping. In the upper-right panel of Figure 2, we present the normalized FFT spectra of the denoised pulse and its residuals, while the lower-right panel displays the normalized FFT spectra of the ACFs of the denoised pulse and its residuals.

8. **Manual intervention:** During data analysis, it remains challenging for automated algorithms to reliably distinguish single pulses exhibiting obvious quasi-periodic characteristics or to determine the most appropriate pulse P_μ when selecting among three different analysis methods, often necessitating manual intervention for accurate judgment. Finally, we plotted the frequency-phase maps for all pulses in which quasi-periodic microstructure were detected, and further excluded the microstructure still affected by RFI through visual inspection.

4. RESULTS

In this section, we present the results of our study on the microstructure in the four inter-pulse pulsars: PSRs J0627+0706, J0826+2637, J0953+0755, and J1946+1805. Using the methods outlined earlier, we determined the τ_μ and P_μ of the microstructure in both MP and IP for each pulsar. The distributions of τ_μ and P_μ are illustrated in Figure 4. Detailed parameters of the microstructure in the MP and IP of these pulsars are provided in Table 3. Figure 10 shows the comparison of microstructure between MP and IP (or PC).

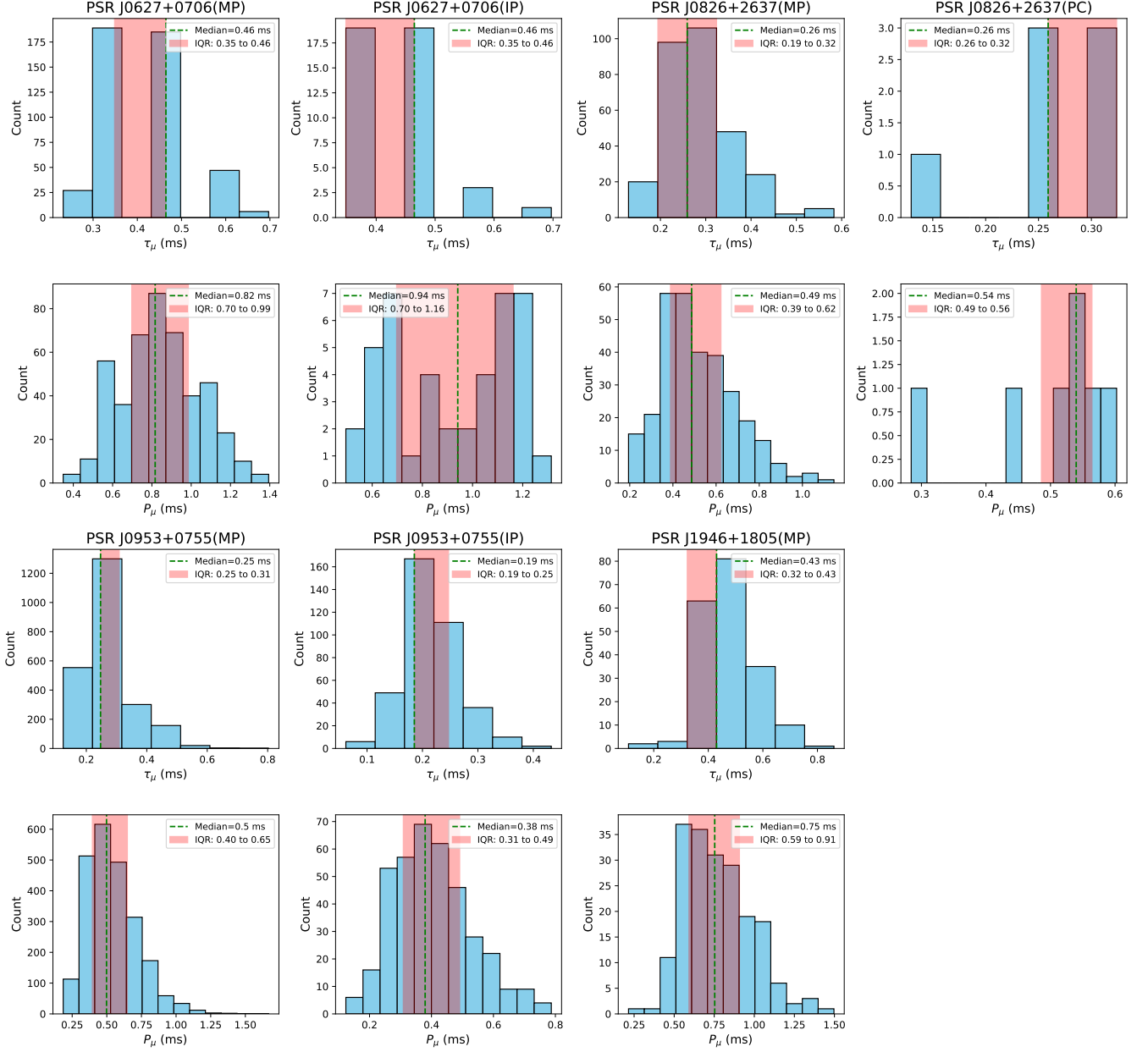


Figure 4. Histograms of τ_μ and P_μ for microstructure in four interpulse pulsars. For each pulsar component, the top panel displays the distribution of τ_μ for quasi-periodic microstructure. And the bottom panel illustrates the distribution of P_μ for quasi-periodic microstructure. In each panel, the green dashed line indicates the median, while the pink shaded region represents the interquartile range (IQR).

4.1. Timescale and Quasi-periodicity of Microstructure

4.1.1. PSR J0627+0706

PSR J0627+0706 was initially identified in the Perseus Arm pulsar survey (currently unpublished), exhibiting a rotational period of approximately 0.476 s (Lower et al. 2020) and a characteristic age ($\tau_c \approx P/(2\dot{P})$) of 0.253 Myr. According to Keith et al. (2010), this pulsar represents an orthogonal rotator, with its MP and IP separated by approximately 180° in longitude, consistent with the upper-left panel in Figure 1. To date, no detailed investigation of the microstructure properties in this pulsar has been conducted.

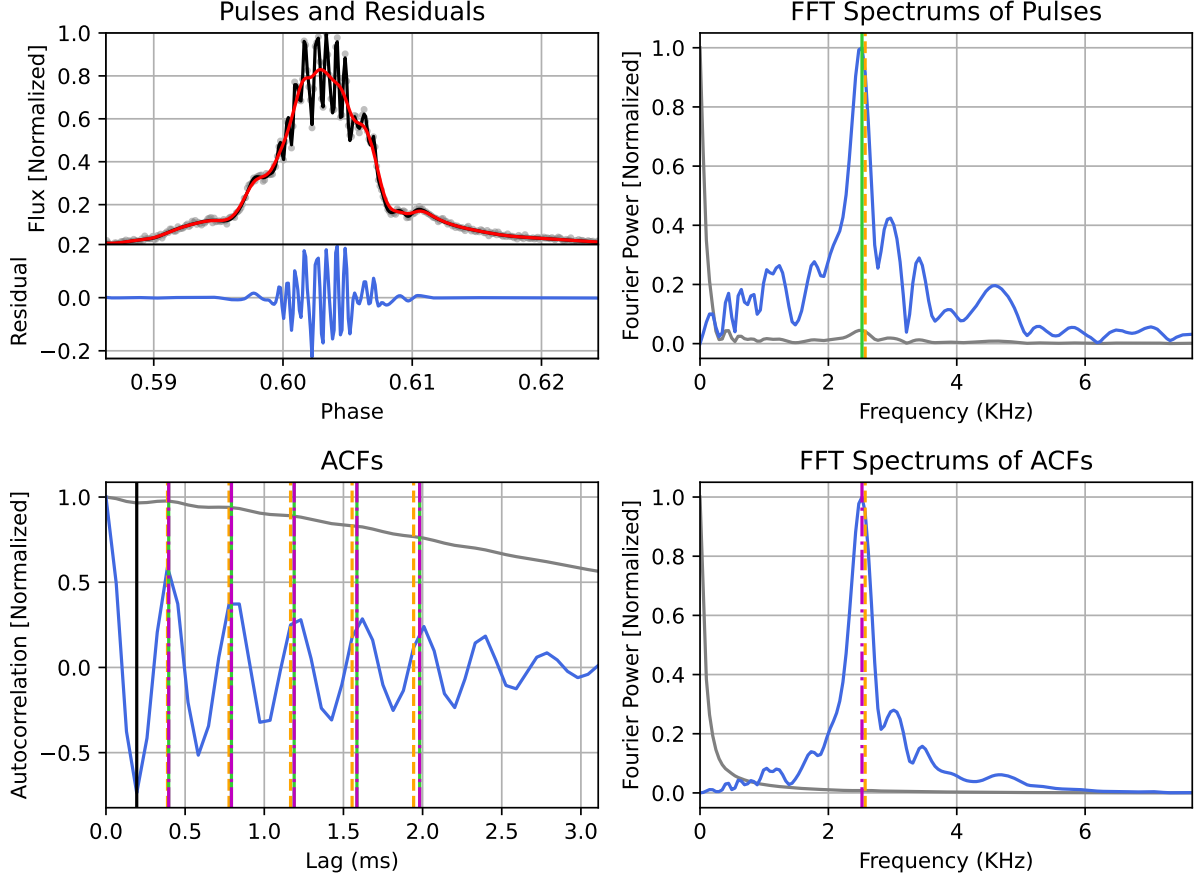


Figure 5. Pulse 185: A representative example of quasi-periodic microstructure observed in the MP of PSR J0826+2637. All other features and annotations follow the same conventions as described in Figure 2.

In the MP component of this pulsar, our analysis revealed quasi-periodic microstructure in 454 pulses out of 1243 high signal-to-noise ratio pulses. Notably, the shortest observed τ_μ in the MP was approximately 0.23 ms, which is comparable to twice the time resolution of our observations. This indicates that the current resolution may be insufficient to fully resolve the smallest microstructure in this pulsar. Furthermore, the minimum P_μ was measured to be ~ 0.35 ms. A representative example of quasi-periodic microstructure (Pulse 136) is presented in Figure 2.

In the IP component of this pulsar, quasi-periodic microstructure was detected in 42 pulses out of 1243 high signal-to-noise ratio pulses. The shortest τ_μ in the IP was measured to be approximately 0.35 ms, which is broader than the corresponding value in the MP (0.23 ms). In addition, the minimum P_μ in the IP is about 0.49 ms, which also exceeds the smallest P_μ observed in the MP. A representative example of quasi-periodic microstructure in the IP (Pulse 212) is illustrated in Figure 3.

4.1.2. PSR J0826+2637 (B0823+26)

PSR J0826+2637 (B0823+26) was first discovered by Craft et al. (1968b), exhibiting a rotation period of approximately 0.531 s (Hobbs et al. 2004) and a characteristic age of ~ 4.92 Myr. The average pulse profile of this pulsar reveals a complex structure, including a MP, an IP, and a post-cursor component (Backer et al. 1973), which is in agreement with the lower-left panel in Figure 1. The IP and MP are separated by approximately 180° in longitude, suggesting a nearly orthogonal emission geometry (Hankins & Fowler 1986). This pulsar exhibits several notable emission properties, including mode-changing, nulling, and periodic fluctuation (Sobey et al. 2015; Hermsen et al. 2018; Basu & Mitra 2019; Chen et al. 2023). The microstructure in this pulsar has been studied by Lange et al. (1998) and M15, with Lange et al. (1998) reporting that the P_μ of the microstructure range from 0.36 ms to 0.66 ms.

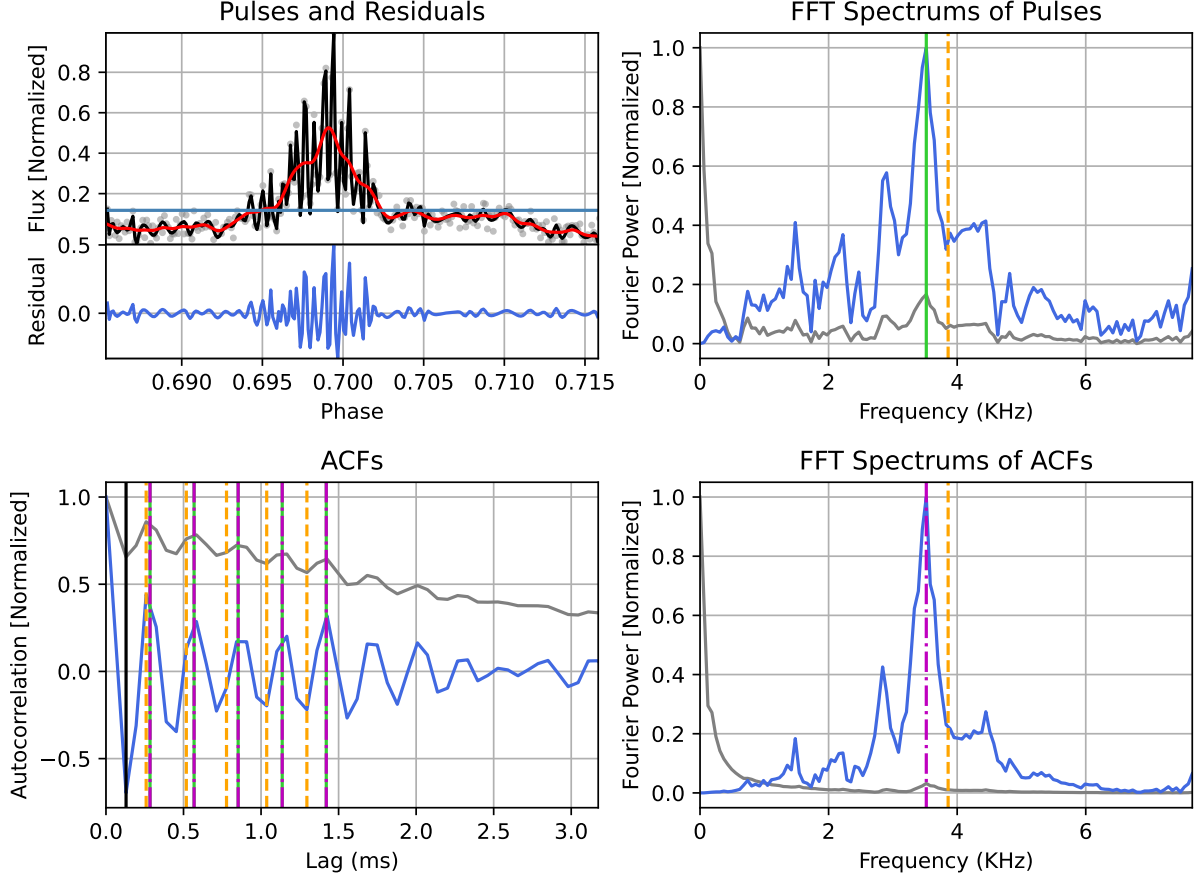


Figure 6. Pulse 157: A representative example of quasi-periodic microstructure observed in the PC of PSR J0826+2637. The light blue horizontal solid line in the top-left panel represent three times the standard deviation of the off-pulse region. All other features and annotations follow the same conventions as described in Figure 2.

In the MP component of this pulsar, quasi-periodic microstructure was detected in 303 pulses out of 648 high signal-to-noise ratio pulses. The shortest τ_μ in the MP was approximately 0.13 ms, corresponding to about two times the time resolution of our observations. Additionally, the minimum P_μ was measured to be 0.19 ms. Our measured $P_\mu = 0.49^{+0.13}_{-0.10}$ ms for the MP component of this pulsar aligns with the previously reported range of 0.36 ms to 0.66 ms in Lange et al. (1998). A representative example of quasi-periodic microstructure (Pulse 185) is illustrated in Figure 5.

Notably, the signal from the IP component was too weak to resolve any microstructure. However, we detected quasi-periodic microstructure in the post-cursor (PC) component of this pulsar for the first time.

In the PC component, quasi-periodic microstructure was detected in only 7 pulses out of 9 high signal-to-noise ratio pulses. The shortest τ_μ in the PC was found to be 0.13 ms, identical to the shortest τ_μ in the MP. Moreover, the minimum P_μ in the PC was measured to be 0.28 ms, which is larger than that in the MP component. A representative example of quasi-periodic microstructure in the PC (Pulse 157) is shown in Figure 6.

Here, we emphasize that the statistical results for quasi-periodic microstructure in the PC component of this pulsar should be interpreted with caution due to the limited sample size (only 7 pulses), which may compromise their statistical significance. Additionally, the shortest observed τ_μ in the MP and PC are only two times the time resolution of our observations, respectively, which suggests the potential existence of even finer microstructure in this pulsar that may not be resolvable with the current observational setup.

4.1.3. PSR J0953+0755 (B0950+08)

PSR J0953+0755 (B0950+08) was first discovered by Pilkington et al. (1968), showing a rotation period of approximately 0.253 s (Hobbs et al. 2004) and a characteristic age of ~ 17.5 Myr. The separation between its MP and IP

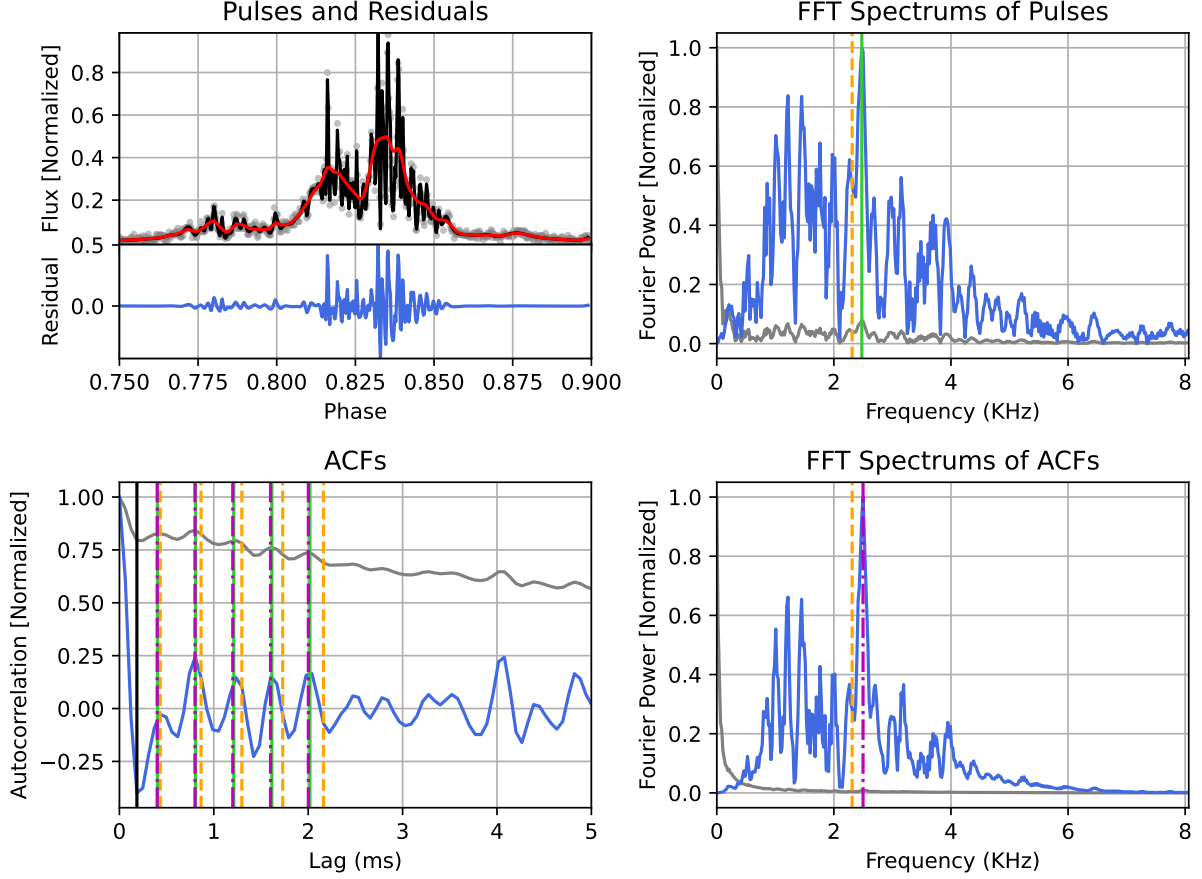


Figure 7. Pulse 3357: A representative example of quasi-periodic microstructure observed in the MP of PSR J0953+0755. All other features and annotations follow the same conventions as described in Figure 2.

remains frequency independent below 5 GHz (Hankins & Cordes 1981), and a bridge component connecting the IP and MP has been detected (Yang et al. 2023), which is in agreement with the upper-right panel in Figure 1. In particular, Wang et al. (2022) successfully detected signals from this pulsar over its entire rotation period using the FAST. The bridge emission and the emission over its entire rotation period indicate that this pulsar has a nearly-aligned emission geometry.

PSR B0950+08 is a well-studied pulsar known for its prominent microstructure features, as reported in numerous studies (Craft et al. 1968a; Hankins 1971b; Hankins & Boriakoff 1978; Cordes 1976; Cordes et al. 1990; Lange et al. 1998; Popov et al. 2002; Kuzmin et al. 2003). At 111.5 MHz, Hankins (1971b) identified quasi-periodic microstructure with P_μ ranging from 0.3 ms to 0.7 ms. Observations at 430 MHz by Hankins & Boriakoff (1978) revealed that the P_μ of microstructure span 0.15 ms to 1.1 ms, with the majority concentrated in the range of 0.4 – 0.6 ms. Furthermore, Lange et al. (1998) measured the τ_μ to be approximately 0.17 ms at 4.85 GHz.

In the MP component of this pulsar, we detected 2334 pulses with quasi-periodic microstructure features out of 4651 high signal-to-noise ratio pulses. The shortest observed τ_μ in the MP was approximately 0.06 ms, which is comparable to the time resolution of our observations. The minimum P_μ was measured to be 0.19 ms. Our measured $P_\mu = 0.50^{+0.15}_{-0.10}$ ms for the MP component of this pulsar aligns with the previously reported range of 0.3 ms to 0.7 ms in Hankins (1971b). A representative example of quasi-periodic microstructure (Pulse 3357) is illustrated in Figure 7.

In the IP component, quasi-periodic microstructure were detected in 381 pulses out of 1021 high signal-to-noise ratio pulses. The shortest τ_μ in the IP was also found to be 0.06 ms, matching the shortest τ_μ in the MP. The minimum P_μ in the IP was measured to be 0.12 ms, which is notably smaller than the corresponding value in the MP. A representative example of quasi-periodic microstructure in the IP (Pulse 3070) is shown in Figure 8.

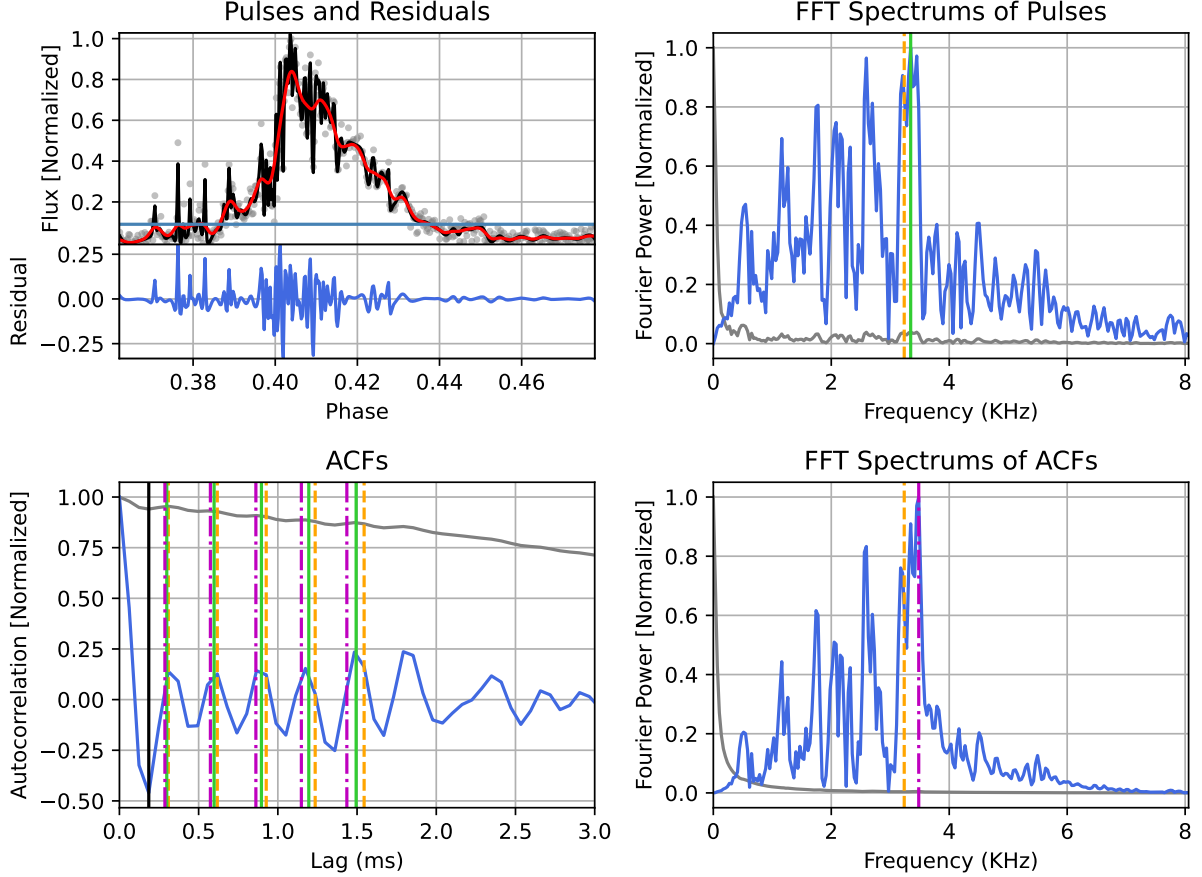


Figure 8. Pulse 3070: A representative example showing quasi-periodic microstructure in IP of PSR J0953+0755. The light blue horizontal solid line in the top-left panel represent three times the standard deviation of the off-pulse region. All other features and annotations follow the same conventions as described in Figure 2.

4.1.4. PSR J1946+1805 (B1944+17)

PSR J1946+1805 (B1944+17) was first discovered by [Vaughan & Large \(1970\)](#), exhibiting a rotation period of approximately 0.44 s ([Hobbs et al. 2004](#)) and a characteristic age of ~ 290 Myr. The average pulse profile of this pulsar, as reported by [Hankins & Fowler \(1986\)](#), consists of a MP and an IP, with weak bridge emission detected between these two components, which is agreement with the lower-right panel in Figure 1. This emission pattern suggests an aligned rotator configuration, where the spin axis is nearly parallel to the magnetic axis, and both the MP and IP originate from the same magnetic pole. In addition to its pulse profile characteristics, this pulsar exhibits several notable emission properties, including nulling, subpulse drifting, and mode-changing ([Deich et al. 1986](#); [Kloumann & Rankin 2010](#); [Tian et al. 2024](#)). Microstructure in this pulsar has been studied by [Cordes et al. \(1990\)](#) and M15, with [Cordes et al. \(1990\)](#) reporting the P_μ of quasi-periodic microstructure of approximately 0.8 ms.

In the MP component of this pulsar, quasi-periodic microstructure was detected in 95 pulses out of 454 high signal-to-noise ratio pulses. The shortest τ_μ in the MP was approximately 0.11 ms, which matches the time resolution of our observations and suggests the potential existence of even finer microstructure that may not be resolvable with the current observational setup. The minimum P_μ was measured to be about 0.22 ms, corresponding to twice the time resolution of our observations. A representative example of quasi-periodic microstructure is illustrated in Figure 9.

Additionally, we attempted to investigate microstructure features in the IP component of this pulsar. However, as shown in Figure 1, due to the exceptionally weak intensity of the IP, no microstructure was detected.

4.2. Comparison of Microstructure in MP and IP

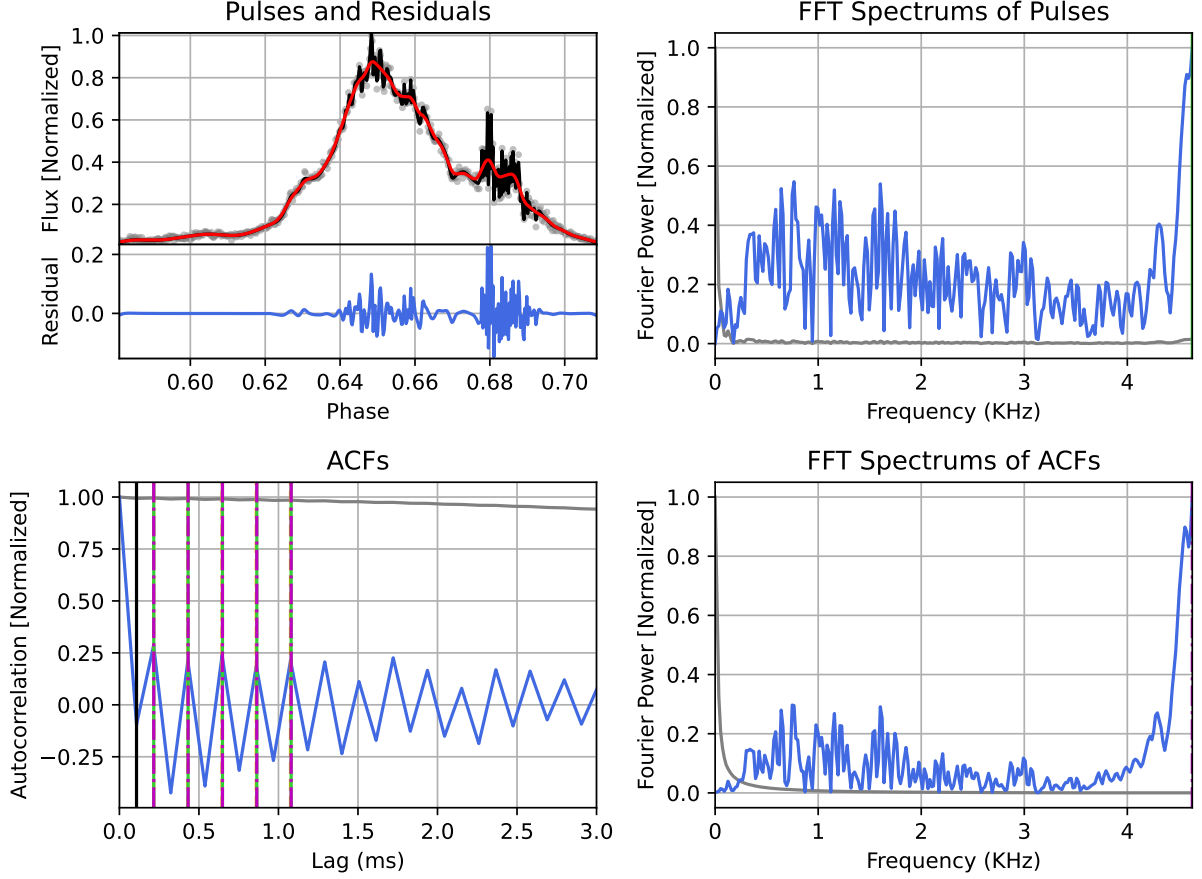


Figure 9. Pulse 400: A representative example of quasi-periodic microstructure observed in the MP of PSR J1946+1805. All other features and annotations follow the same conventions as described in Figure 2.

In this subsection, we focus on comparing the similarities and differences between microstructure in MP and IP (PC). In Figure 10, the horizontal coordinate is the rotation period, and the results of τ_μ and P_μ of quasi-periodic microstructure within are shown in the top panel and the bottom panel, respectively. The results demonstrate that the τ_μ and P_μ of quasi-periodic microstructure across different pulse components show consistency within their respective error ranges.

To further confirm this result and explore the potential correlations between IP (PC) and different components of MP, we filtered out quasi-periodic microstructure that occur simultaneously in a single pulse. We detected the simultaneous occurrence of MP and IP (or PC) in 17, 3, and 190 single pulses for PSRs J0627+0706, J0826+2637 and J0953+0755, respectively. Additionally, we statistically analyzed the τ_μ and P_μ distributions of these microstructure in PSRs J0627+0706 and J0953+0755. As shown in Figure 11, the τ_μ and P_μ of simultaneously occurring microstructure with different components in PSR J0627+0706 remain consistent within error margins. However, we noted that in PSR J0953+0755, both the τ_μ and P_μ of microstructures in IP are relatively smaller than those in MP.

Furthermore, to quantify the differences in τ_μ and P_μ between simultaneously occurring microstructure of different components within the same sub-pulses, we defined $\Delta\tau_\mu = \tau_\mu^{MP} - \tau_\mu^{IP}$ and $\Delta P_\mu = P_\mu^{MP} - P_\mu^{IP}$. The two-dimensional distributions of parameters $\Delta\tau_\mu$ and ΔP_μ for PSRs J0627+0706 and J0953+0755 are shown in Figures 12 and 13, respectively. Kernel density estimates are overlaid on the scatter panels. Two blue solid lines (horizontal and vertical) represent the medians of $\Delta\tau_\mu$ and ΔP_μ , respectively. The results show that the differences in τ_μ and P_μ between simultaneously occurring microstructure of MP and IP within the same sub-pulses of PSR J0627+0706 are not significant. However, these differences are relatively evident in PSR J0953+0755. It should be noted that the median of $\Delta\tau_\mu$ exactly corresponds to the time resolution of this pulsar, and the median of ΔP_μ corresponds to twice the

time resolution. Further investigation into this difference in the microstructure of this pulsar may require further improvement of the time resolution of observation.

Here, we have to point out that the small sample size and the limit of time resolution of observations may cause our results to be somewhat unrepresentative. Therefore, we look forward to more observations of the microstructure of interpulse pulsars, which will help us further understand the similarities and differences between microstructure in MP and IP (or PC).

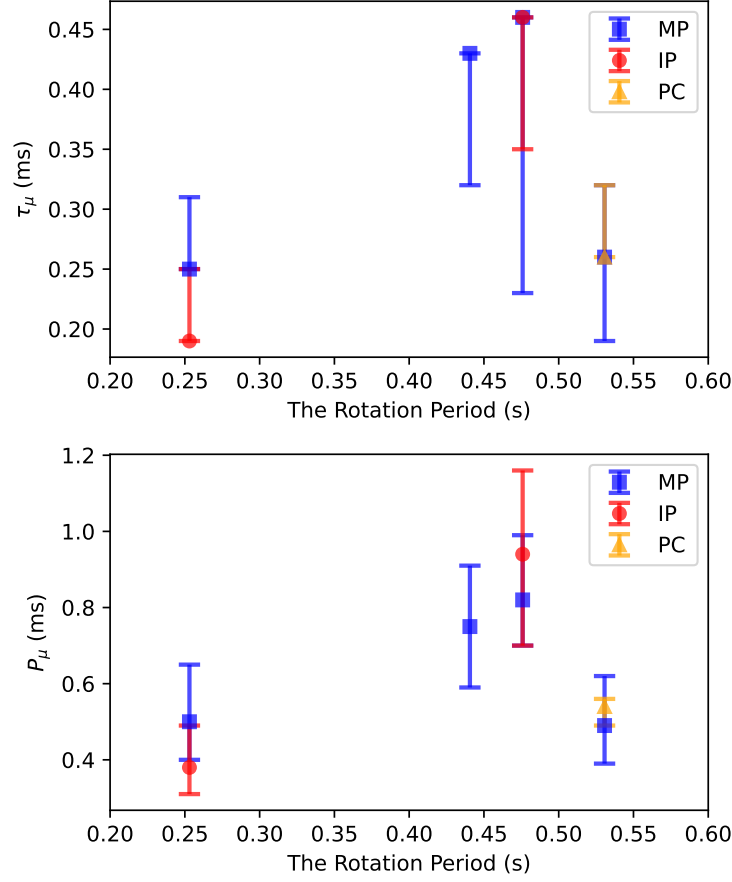


Figure 10. The horizontal coordinate is the rotation period. The results of τ_μ and P_μ of quasi-periodic microstructure are shown in the top panel and the bottom panel, respectively. The blue, the red and the orange dots represent the results of the MP, IP and PC components, respectively.

4.3. The Relationship between the Rotation Periods and Periods of Quasi-periodic Substructures

The rotation period and the quasi-periodic substructure ($P - P_\mu$) relation of microstructures in neutron star populations (such as, normal pulsars, magnetars, long-rotation-period pulsars, MSPs and RRATs) has been widely studied (Kramer et al. 2024). However, whether all pulsars follow this relation remains uncertain and requires investigation with a larger sample to be confirmed. By compiling previous data and incorporating new measurements from this work, we attempt to re-examine the $P - P_\mu$ relationship.

For magnetars, we cite the median of P_μ of magnetars in (Kramer et al. 2024), including: PSR J1622–4950, XTE J1810–197, Swift J1818.0–1607 and GLEAM–X J162759.5–523504.3. For normal pulsars, data were mainly collected from M15 and this study. The data cited from M15 was obtained using smoothing bandwidths of $0.075 \times N_{bin}$, and only that from the stronger integrated profile component was considered for the pulsars whose microstructure in different components were investigated (see M15 for details). Similarly, we only considered the microstructure data from the MP component in this work. For MSPs, we cite the results of all four MSPs in (De et al. 2016) and (Liu et al. 2022),

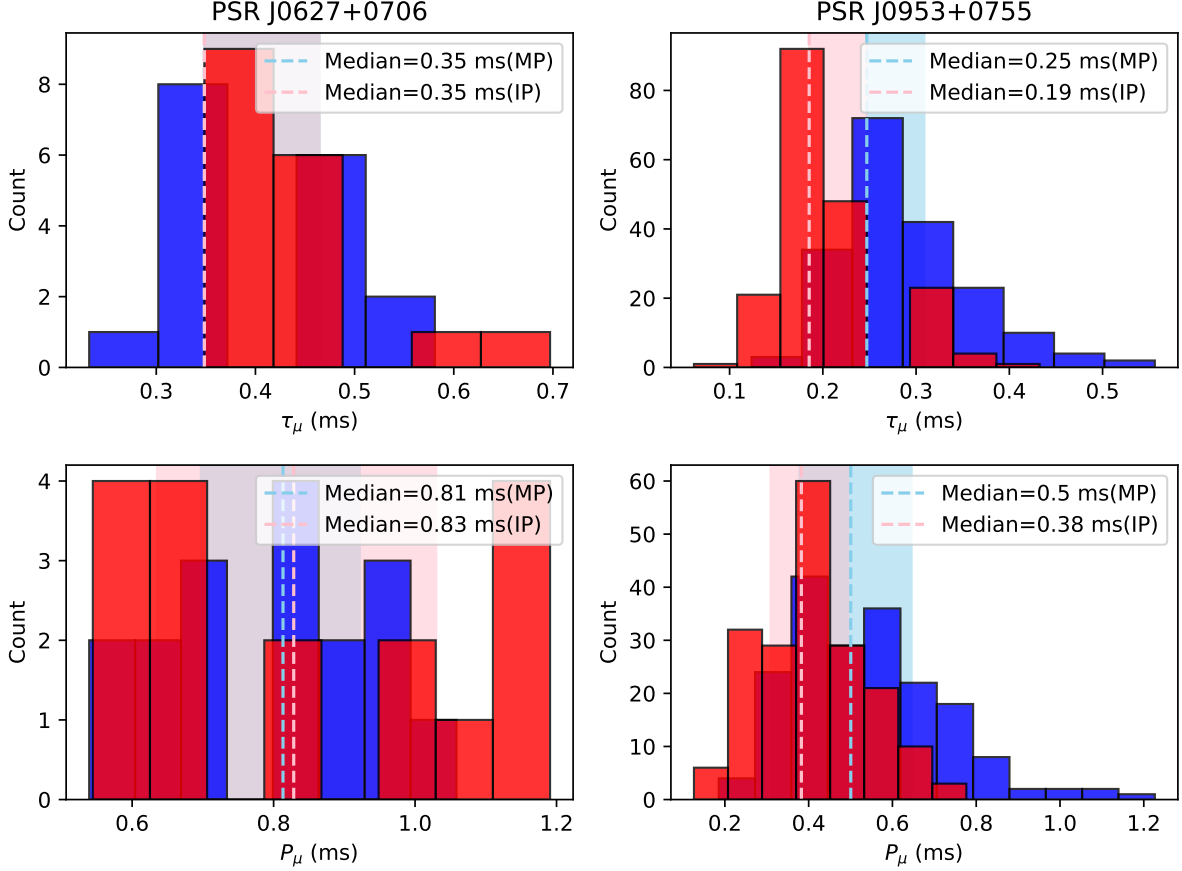


Figure 11. Histograms of τ_μ and P_μ for microstructure that occur simultaneously in single pulses in two interpulse pulsars. For each pulsar, the top panel displays the distribution of τ_μ for quasi-periodic microstructure in MP (blue) and IP (or PC) (red), respectively. And the bottom panel illustrates the distribution of P_μ for these quasi-periodic microstructure. In each panel, the dashed line indicates the median value, while the shaded region represents the interquartile range (IQR).

including MSPs J0437–4715, J2145–0750, J1022+1001 and J1744–1134. For long-rotation-period pulsars, we cite the results of PSRs J1744–1134 (Mitra et al. 2020) and J0901-4046 (Caleb et al. 2022a). Caleb et al. (2022a) detected the quasi-periodic microstructure in PSR J0901–4046 with the rotation period of about 76 s, and reported the median $\tau_\mu = 49$ ms, the error of τ_μ about 11 ms and the relationship between P_μ and τ_μ : ($\tau_\mu = 0.3782 \times P_\mu + 11.07$), but they did not provide the median of P_μ . So we can only give a rough estimate of P_μ from the above relation and the median of τ_μ : $P_\mu = 100 \pm 29$ ms. Moreover, As far as we know, microstructure in only three RRATs have been studied, but we just use only three data from these RRATs for fitting (Dang et al. 2024; Zhong et al. 2024; Tang et al. 2025), because Chen et al. (2022) only provided the P_μ ($\approx 2.31 \pm 0.25$ ms) of an example of the quasi-periodic microstructure of RRAT J1918–0449, without statistical results of all quasi-periodic microstructure. Dang et al. (2024) gave the median P_μ (≈ 0.91 ms) for the quasi-periodic microstructure in RRAT J0139+3336. Zhong et al. (2024) provided the mean value of $P_\mu \approx 1.56$ ms in RRAT J1913+1330. Based on the study by Tang et al. (2025), we determined a median P_μ of 0.26 ms for the 12 quasi-periodic microstructure, with the interquartile range (0.25 – 0.30 ms) representing the measurement uncertainty. Additionally, we noticed the quasi-periodic microstructure in RRAT J1913+1330 in Zhang et al. (2024), although they did not conduct an in-depth analysis of the quasi-periodicity of microstructure. In addition, periods of these RRATs were cited from the RRATalog⁴. In summary, our dataset for fitting includes magnetars, normal pulsars, long-rotation-period pulsars, MSPs and RRATs, as shown in Table 4.

⁴ <https://rratalog.github.io/rratalog/>

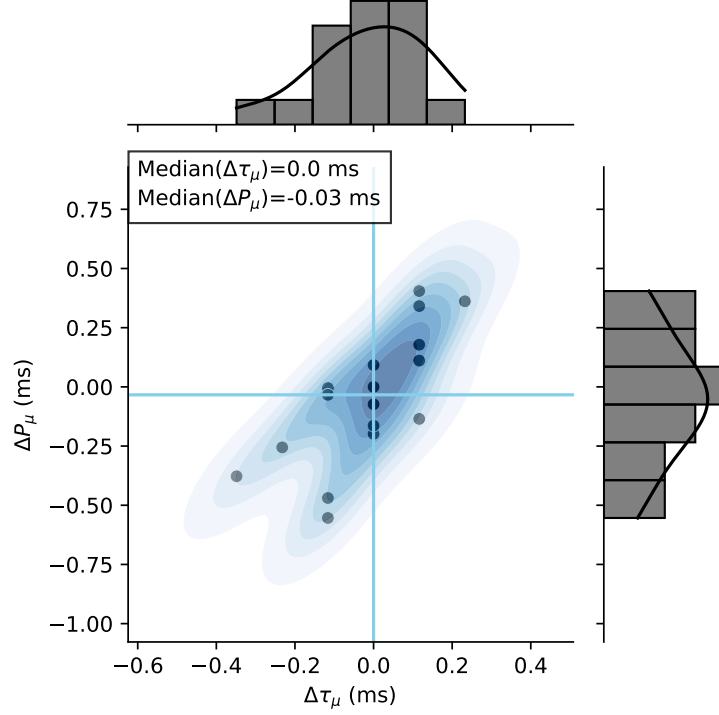


Figure 12. The distribution of $\Delta\tau_\mu$ and ΔP_μ in PSR J0627+0706. The black scatter points represent the distribution of $\Delta\tau_\mu$ and ΔP_μ , the blue shaded area is the two-dimensional kernel density estimation (KDE), and the sky-blue solid lines denote the medians of the of $\Delta\tau_\mu$ and ΔP_μ , respectively; the values in the text box at the upper left corner are the specific measured values of the corresponding medians (retained to two decimal places).

Due to the significant differences in magnitude spanning multiple orders of magnitude within the data, directly applying the least squares method to fit the power function model $P_\mu = A \times P^\alpha$ might lead to substantial errors. Therefore, we adopt a logarithmic transformation approach for processing: First, we perform a logarithmic conversion on the original data to obtain $\ln(P)$ and $\ln(P_\mu)$. Then, based on the linearized model $\ln(P_\mu) = \ln(A) + \alpha \ln(P)$, we utilize the least squares method to conduct a linear fit on the transformed data. Finally, we convert the fitting results back to the original form of the power function. During this process, the errors of the model parameters are precisely calculated through the error propagation formula to ensure the accuracy and reliability of the results. As shown in Figure 14, we confirm a linear dependency on rotational period: $P_\mu(\text{ms}) = (1.337 \pm 0.114) \times P(\text{s})^{(1.063 \pm 0.038)}$.

In addition, We have noted some reports on quasi-periodic substructures in FRBs in recent years, including FRBs 20200120E (Majid et al. 2021), 20191221A, 20210206A, 20210213A (Chime/Frb Collaboration et al. 2022), 20201020A (Pastor-Marazuela et al. 2023) and 20201124A (Niu et al. 2022) (see Table 5 for details). In recent years, numerous theoretical models have been proposed to explain the radiation mechanisms of FRBs, while an increasing number of studies have focused on identifying their potential host stars (Bochenek et al. 2020; CHIME/FRB Collaboration et al. 2020). Magnetars are leading candidate sources of FRBs (Lyubarsky 2014; Beloborodov 2017). As shown in Figure 14, the quasi-periodic substructure within magnetars exhibits an approximately the linear relationship between P_μ and P . If the radiation mechanism of the quasi-periodic substructures in FRBs is similar to that in other neutron stars, or if FRBs indeed originate from magnetars, then according to the periods of the quasi-periodic substructures in FRBs and our fitting results, we can roughly predict the spin periods of the FRBs' host stars (P_F), as shown in Table 5. In addition, we note that FRB 20201124A listed in Table 5 is a repeating FRB, and suggest that quasi-periodic substructures in repeating FRBs may provide valuable insights for periodicity searches in these repeaters. However, as shown in Figure 14, the predicted rotational periods (< 1 s) of the host stars of FRBs 20200120E and 20201020A show statistically are much smaller than typical magnetar periods, which may suggest a non-unified origin scenario for FRBs or this method of inferring the host star's rotational period through measurements of quasi-periodic microstructure

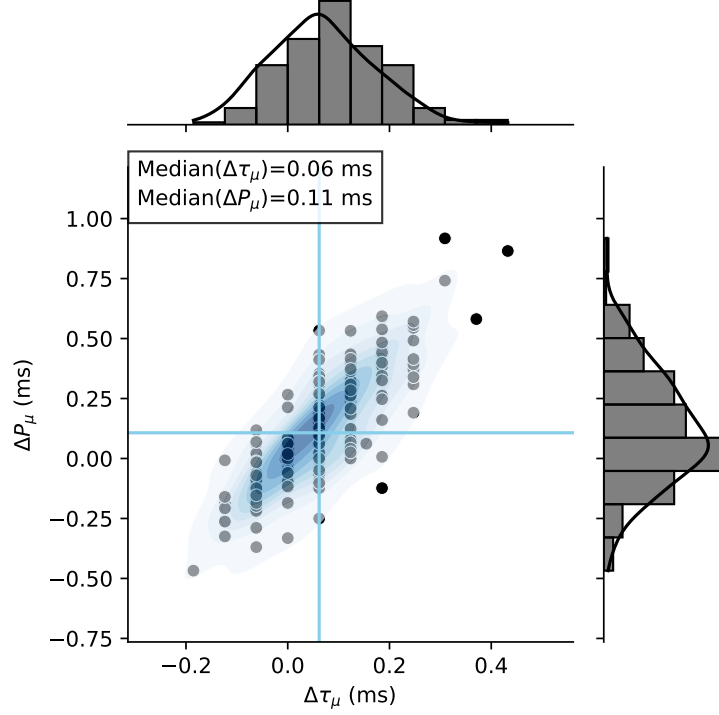


Figure 13. The distribution of $\Delta\tau_\mu$ and ΔP_μ in PSR J0953+0755. Others are the same with that in Figure 12.

is unreliable. We look forward to future studies confirming that the host stars of these FRBs are consistent with our results, and anticipate detecting quasi-periodic substructures in more FRBs, particularly in repeating FRBs.

4.4. Morphological Analysis of Single-pulses

During the data processing, we noticed some interesting single-pulse morphologies. In this section, we focus on analyzing the morphology of single-pulses, which exhibit significant variability both across different epochs and within individual epochs, while certain characteristic features remain persistent. Following the classification scheme proposed by Caleb et al. (2022a), single pulses can be categorized into seven distinct types: normal, quasi-periodic, spiky, double-peaked, partially nulling, split-peak, and triple-peaked, as illustrated in Figure 2 of Caleb et al. (2022a). Notably, partially nulling pulses represent a distinctive phenomenon marked by an abrupt cessation of pulse intensity at specific phases. However, we emphasize that this classification is not strictly rigid or mutually exclusive. In particular, we observed that quasi-periodic features can coexist with partially nulling pulses as well as with pulses exhibiting multiple peaks (e.g., double-peaked or triple-peaked pulses), suggesting a continuum of pulse morphologies influenced by complex underlying physical processes.

To further explore the diversity of pulse characteristics, we also performed a classification based on the presence or absence of low-frequency envelope features. In the following subsections, we analyzed the morphological properties of single pulses for each pulsar in our sample. This investigation aims to uncover patterns and variations in pulse morphology, which may provide critical insights into the physical mechanisms governing pulse emission processes.

PSR J0953+0755: In the MP of this pulsar, we observed various single-pulse morphologies, including those with low-frequency envelopes (top panels of Figure 15) and those without (bottom panels of Figure 15). Notably, our analysis revealed not only partially nulling pulses but also instances where partial-nulling structures and quasi-periodic microstructure coexist within individual pulses, as illustrated in the panels of Figure 16. Additionally, we find that certain nulling pulses maintain consistent pulse profiles before and after the nulling phase, as depicted in the top four panels of Figure 16. In contrast, other partially nulling pulses undergo significant changes in their pulse profiles following the nulling phase, as demonstrated in the bottom four panels of Figure 16, in which, these post-nulling pulse components display quasi-periodic microstructure without low-frequency envelopes.

Table 4. Dataset for fitting the relation between the rotation periods and periods of quasi-periodic substructures

Name	Type	P (s)	P_μ (ms)	Reference
PSR J1622–4950	Magnetar	4.326	10.0(0.2)	(Kramer et al. 2024)
XTE J1810–197	Magnetar	5.540	12.0(0.06)	(Kramer et al. 2024)
Swift J1818.0–1607	Magnetar	1.364	2.24(0.04)	(Kramer et al. 2024)
GLEAM-X J162759.5–523504.3	Magnetar	1091.169	6110(290)	(Kramer et al. 2024)
J0437–4715	MSP	0.005757	0.004(0.00079)	(De et al. 2016)
J2145–0750	MSP	0.016052	0.01536(0.00177)	(De et al. 2016)
J1022+1001	MSP	0.016453	$0.0149^{+0.0052}_{-0.0028}$	(Liu et al. 2022)
J2145–0750	MSP	0.016052	$0.0178^{+0.0027}_{-0.0032}$	(Liu et al. 2022)
J1744–1134	MSP	0.004075	$0.006^{+0.0024}_{-0.0008}$	(Liu et al. 2022)
J2144–3933	Long-rotation-period Pulsar	8.510	11.8(5.83)	(Mitra et al. 2020)
J0901–4046	Long-rotation-period Pulsar	75.886	100(29)*	(Caleb et al. 2022a)
J0139+3336	RRAT	1.248	0.91	(Dang et al. 2024)
J1913+1330	RRAT	0.923	1.56	(Zhong et al. 2024)
J1913+1330	RRAT	0.923	$0.26^{+0.04}_{-0.01}$	(Tang et al. 2025)
B0301+19(–2.2°–2.5°)	Normal Pulsar	1.387	1.19(0.44)	(Mitra et al. 2015)
B0525+21(–2.85°–2.86°)	Normal Pulsar	3.745	3.57(1.76)	(Mitra et al. 2015)
J0546+2441	Normal Pulsar	2.843	2.38(0.71)	(Mitra et al. 2015)
J0659+1414	Normal Pulsar	0.384	0.42(0.09)	(Mitra et al. 2015)
J0754+3231	Normal Pulsar	1.442	2.10(0.98)	(Mitra et al. 2015)
J0826+2637	Normal Pulsar	0.530	0.72(0.45)	(Mitra et al. 2015)
J0837+0610(–1.32°–1.46°)	Normal Pulsar	1.275	0.72(0.18)	(Mitra et al. 2015)
J0953+0755	Normal Pulsar	0.253	0.63(0.22)	(Mitra et al. 2015)
J1136+1551(–1.47°–3.39°)	Normal Pulsar	1.187	0.83(0.44)	(Mitra et al. 2015)
J1239+2453	Normal Pulsar	1.382	2.16(1.16)	(Mitra et al. 2015)
J1740+1000	Normal Pulsar	0.154	0.48(0.18)	(Mitra et al. 2015)
J1740+1311	Normal Pulsar	0.803	1.80(0.80)	(Mitra et al. 2015)
J1910+0714	Normal Pulsar	2.712	5.36(2.21)	(Mitra et al. 2015)
J1912+2104	Normal Pulsar	2.233	4.40(2.12)	(Mitra et al. 2015)
J1921+2153(–2.45°–3.10°)	Normal Pulsar	1.337	1.31(0.62)	(Mitra et al. 2015)
J1932+1059	Normal Pulsar	0.226	0.48(0.18)	(Mitra et al. 2015)
J1946+1805	Normal Pulsar	0.440	0.71(0.18)	(Mitra et al. 2015)
J2004+3137	Normal Pulsar	2.111	1.25(0.53)	(Mitra et al. 2015)
J2018+2839	Normal Pulsar	0.557	0.66(0.18)	(Mitra et al. 2015)
J2022+2854(–3.78°–1.21°)	Normal Pulsar	0.343	0.48(0.18)	(Mitra et al. 2015)
J2037+1942	Normal Pulsar	2.074	3.10(1.50)	(Mitra et al. 2015)
J2113+2754	Normal Pulsar	1.202	1.13(0.09)	(Mitra et al. 2015)
J2317+2149	Normal Pulsar	1.444	1.01(0.09)	(Mitra et al. 2015)
J0627+0706(MP)	Normal Pulsar	0.476	$0.82^{+0.17}_{-0.12}$	This Work
J0826+2637(MP)	Normal Pulsar	0.531	$0.49^{+0.13}_{-0.10}$	This Work
J0953+0755(MP)	Normal Pulsar	0.253	$0.50^{+0.15}_{-0.10}$	This Work
J1946+1905(MP)	Normal Pulsar	0.441	$0.75^{+0.16}_{-0.16}$	This Work

NOTE—Columns 1 and 2 list the name and the type of stars, respectively. Column 3 and 4 provide periods of the rotation periods and the characteristic periods of quasi-periodic substructure, respectively. Reference are list in the last column. The characteristic period marked with asterisk (*) for PSR J0901–4046 indicates rough estimate based on the method described in the main text. The data cited from M15 was obtained using smoothing bandwidths of $0.075 \times N_{bin}$, and only that from the stronger integrated profile component was considered for the pulsars (marked longitude ranges in the table) whose microstructure in different components were investigated (see M15 for details).

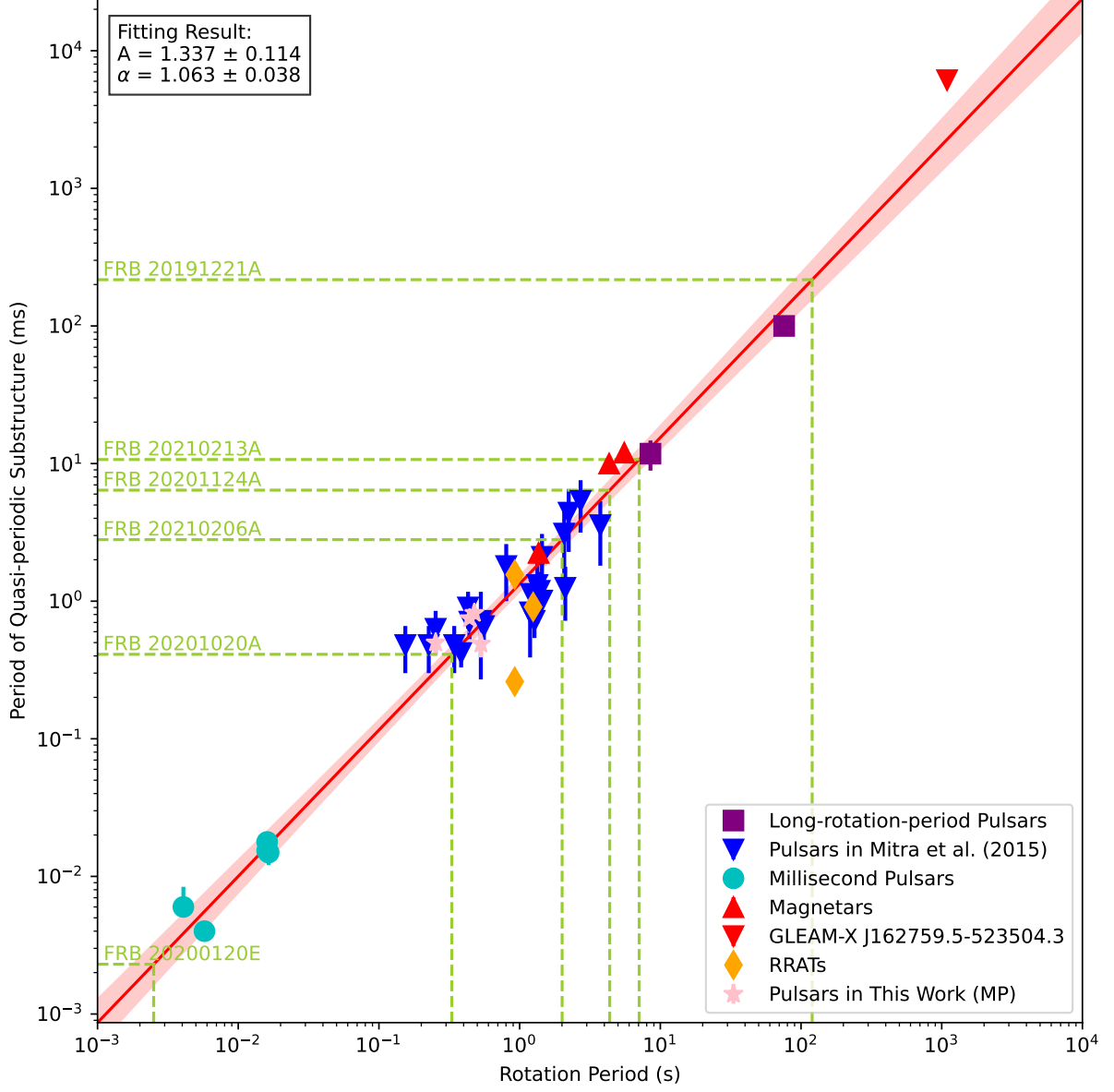


Figure 14. The relationship between the rotation periods and periods of quasi-periodic substructures. A power function $P_\mu = A \times P^\alpha$ is used to fit these data points, where P is in second. The fitting result is $P_\mu(\text{ms}) = (1.337 \pm 0.114) \times P(\text{s})^{(1.063 \pm 0.038)}$. The error interval of 3σ is also shown in this figure.

Beyond the partially nulling pulses characterized by an abrupt intensity drop, we identified a subset of pulses exhibiting rapid intensity increases (Pulses 307 and 332) or sharp decays, as illustrated in Figure 17. Notably, the abrupt increases or decreases in the intensity of these single pulses shown in this figure all occur near a phase of 0.83, which may imply an unrecognized physical mechanism. However, whether this phenomenon is a coincidence still needs to be verified through further research.

In the IP of this pulsar, almost all pulses exhibiting quasi-periodic microstructure are superimposed on low-frequency envelopes, as demonstrated in Figure 18. Furthermore, our analysis of the IP has also revealed the presence of both partially nulling pulses and pulses exhibiting rapid intensity increases, as shown in Figure 19.

PSRs J0627+0706, J0826+2637 and J1946+1805: In these three pulsars, we did not detect any quasi-periodic microstructure without low-frequency envelopes. Furthermore, no significant partially nulling pulses or pulses exhibiting rapid intensity increase or sharp decay were observed. This suggests that partially nulling pulses, quasi-

Table 5. Information about Quasi-periodic substructures in FRBs

NAME	P_μ (ms)	Reference	P_F (s)
20191221A	216.8 ± 0.1	Chime/Frb Collaboration et al. (2022)	122 ± 22
20200120E	0.0023	Majid et al. (2021)	0.0023 ± 0.0005
20201020A	0.411	Pastor-Marazuela et al. (2023)	0.328 ± 0.029
20201124A	$6.409^{+3.327*}_{-1.540}$	Niu et al. (2022)	$4.37^{+3.2}_{-1.4}$
20210206A	2.8 ± 0.1	Chime/Frb Collaboration et al. (2022)	2.02 ± 0.18
20210213A	10.7 ± 0.1	Chime/Frb Collaboration et al. (2022)	7.07 ± 0.76

NOTE—Column 1 lists the name of FRBs. Column 2 provides periods of quasi-periodic substructure in these FRBs. Reference are list in Column 3. The predicted rotational periods of the host stars for these FRBs are listed in the last column. It should be noted that the characteristic period of quasi-periodic substructures in FRB 20201124A (marked with a superscript *) are represented by their median values, with uncertainties determined from the upper and lower quartiles.

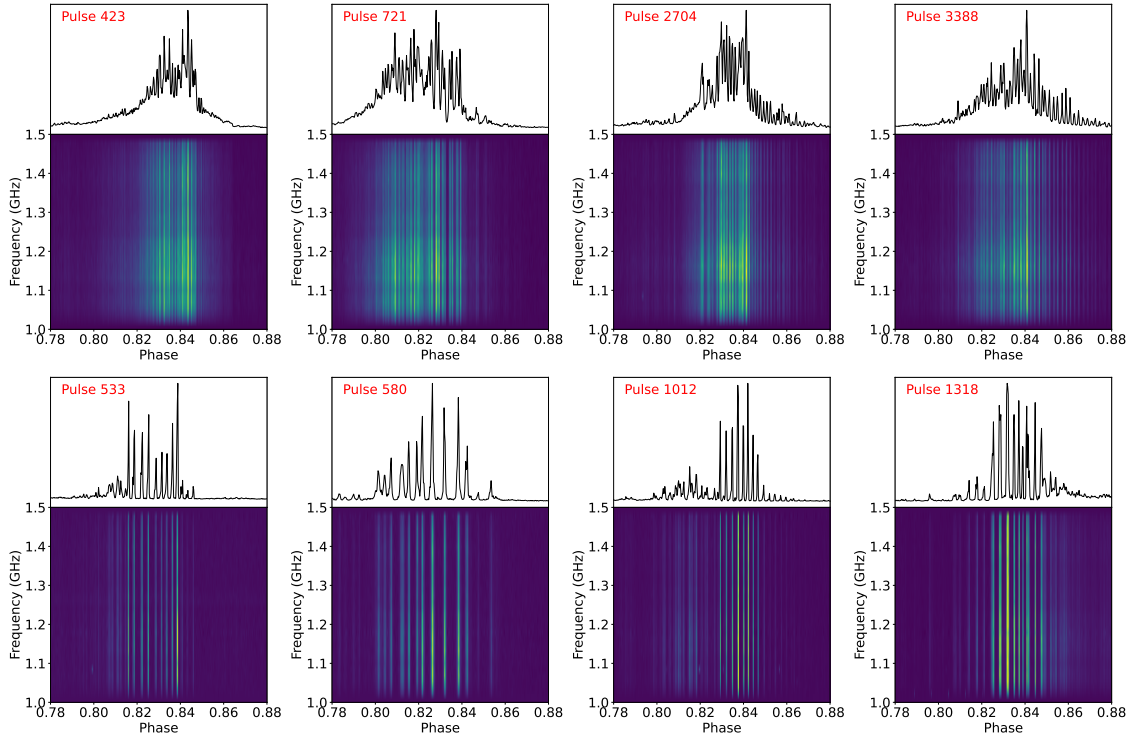


Figure 15. Gallery of quasi-periodic microstructure in the MP of PSR J0953+0755. Each panel features a pulse profile (top) and a phase-frequency intensity map (bottom), with data downsampled to 32 frequency channels.

periodic microstructure without low-frequency envelopes, and pulses with rapid intensity variations may not be common phenomena within the pulsar population.

We propose that partial nulling phenomena may arise from the line of sight sweeping through gaps between sub-beamings. The phase inconsistency in partial nulling may be explained by variations in sub-beamings caused by fluctuations in plasma density. Note that although we report these interesting single-pulse morphologies in this paper, they are not the focus here. Therefore, we refrain from conducting a systematic analysis in this study and will pursue in-depth investigations in subsequent research.

5. DISCUSSION

5.1. Physical Origin of Microstructure

Table 6. The Lorentz Factors (γ) of Pulsars Derived from Microstructure

NAME	P (s)	τ_μ (ms)	Reference	ζ	Reference	γ
J1022+1001	0.01645	0.009 ± 0.001	Liu et al. (2022)	7.9(1.4)	Fiore et al. (2024)	2116.5
J1932+1059	0.226	$0.24(0.09)^*$	Mitra et al. (2015)	$54.32^{+2.21}_{-2.28}$	Sun et al. (2025)	184.5
J2144–3933	8.510	5.9(2.91)	Mitra et al. (2020)	72.03	Mitra et al. (2020)	241.3
J0953+0755	0.253	$0.25^{+0.06}_{-0.00}$	This Work	$178.49^{+4.68}_{-3.90}$	Sun et al. (2025)	6112.2
J1946+1805	0.441	$0.43^{+0.00}_{-0.11}$	This Work	$170.25^{+4.83}_{-5.74}$	Sun et al. (2025)	963.8

NOTE—Columns 1 and 2 list the pulsar name and its rotation period, respectively. Columns 3 and 4 present the characteristic timescales of microstructure and their corresponding references. Columns 5 and 6 provide the ζ values and their associated references, respectively. The derived Lorentz factors (γ) are listed in the final column. τ_μ of PSR J1932+1059 is an approximate estimate obtained by halving the characteristic period of microstructure reported in M15.

The physical origin of pulsar microstructure is an important question in understanding the mechanisms of radio emission of pulsars. Current theories can be broadly categorized into geometric beaming effects, temporal/radial modulation effects, plasma instabilities, and coherent radiation mechanisms, as detailed below:

Angular Beaming and Relativistic Particle Flux Tubes: A leading paradigm posits that microstructure arises from narrow flux tubes of relativistic charged particles streaming along curved magnetic field lines, whose radiation is beamed in their direction of motion. As the pulsar rotates, these beams sweep across the observer’s line of sight, with the width of the microstructure reflecting the width of the angular beam (Benford 1977; Bartel et al. 1980). A point source moving with relativistic energy emits radiation that is beamed in the direction of its motion. If assuming that the fine structure is a consequence of a flux tube, which consists of such point sources, sweeping across our line of sight, then, under the assumption that the flux tube is infinitely narrow, we can deduce a lower bound for the particle

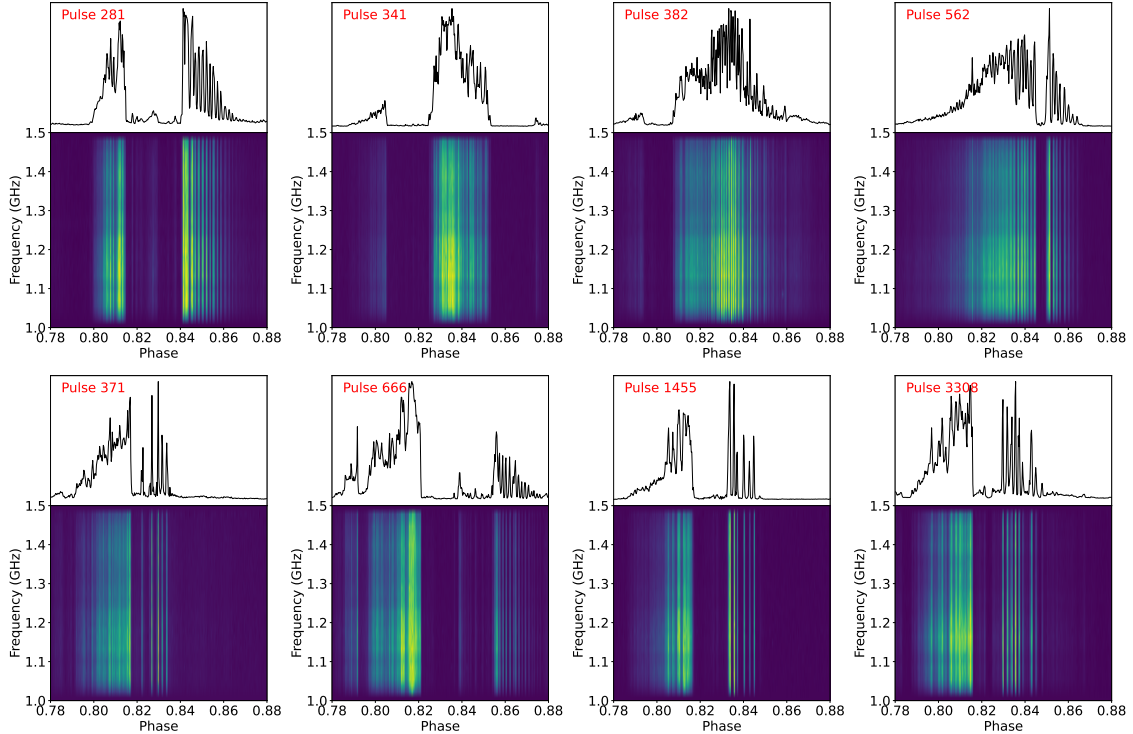


Figure 16. Gallery of partially nulling pulses in the MP of PSR J0953+0755. Each panel features a pulse profile (top) and a phase-frequency intensity map (bottom), with data downsampled to 32 frequency channels.

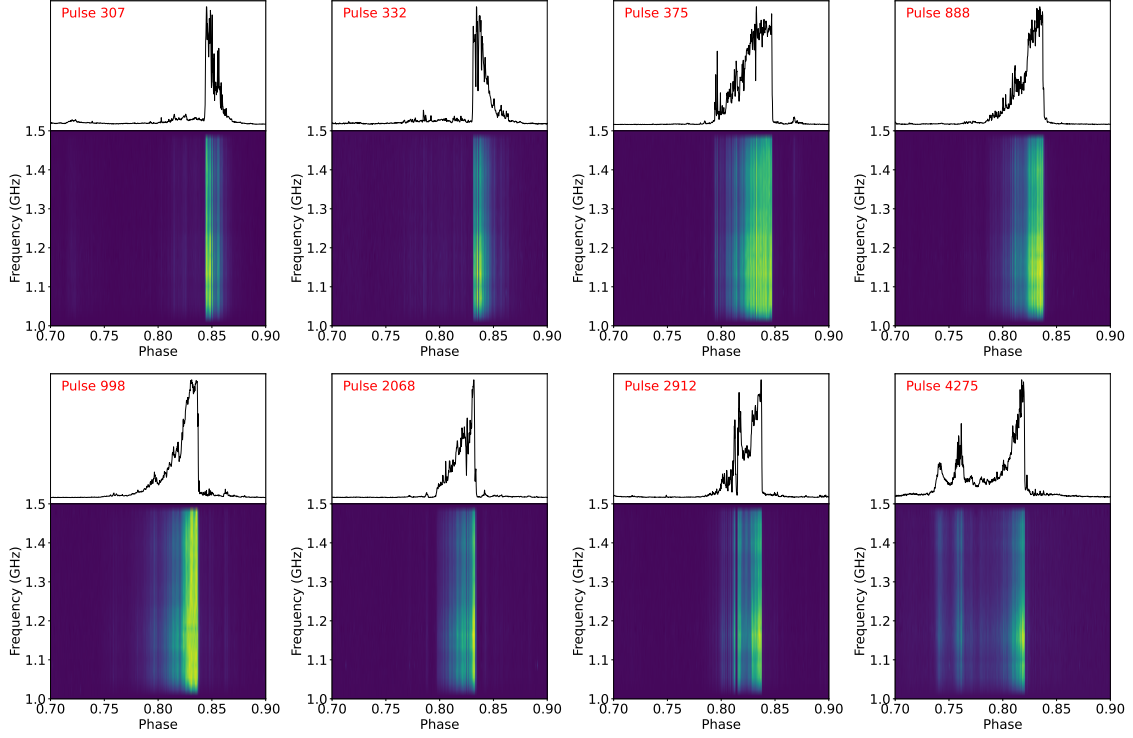


Figure 17. Gallery of pulses exhibiting rapid intensity increase or sharp decay in the MP of PSR J0953+0755. Each panel features a pulse profile (top) and a phase-frequency intensity map (bottom), with data downsampled to 32 frequency channels.

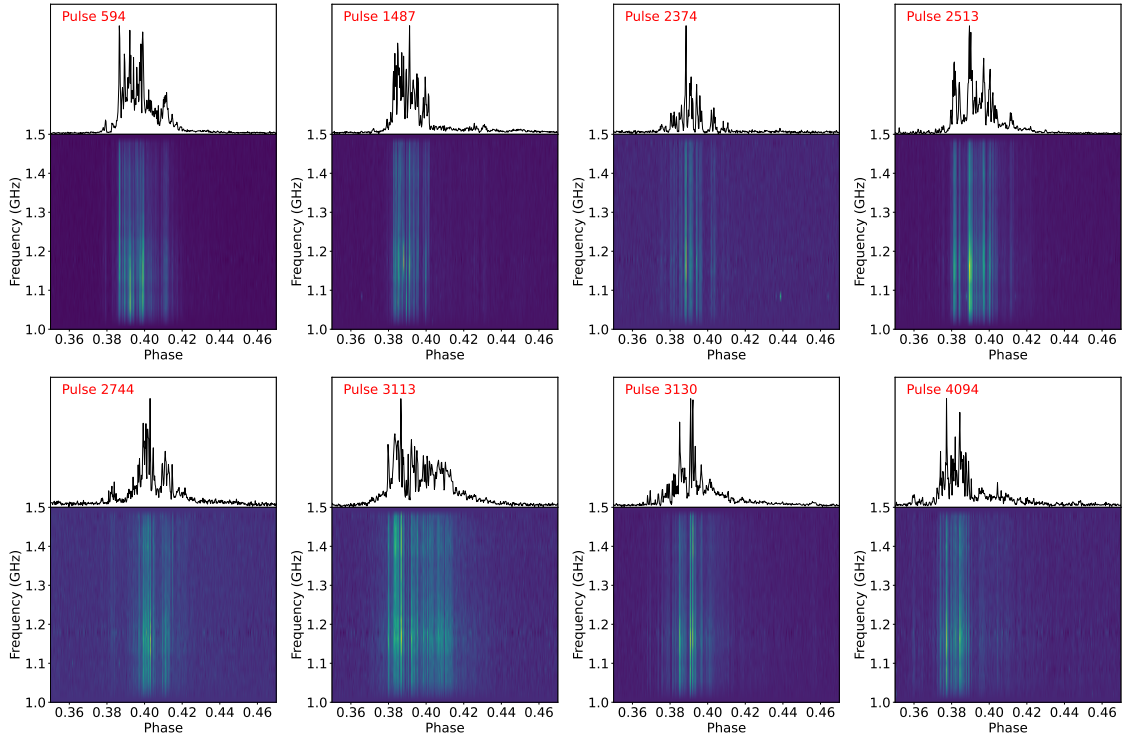


Figure 18. Gallery of quasi-periodic microstructure in the IP of PSR J0953+0755. Each panel features a pulse profile (top) and a phase-frequency intensity map (bottom), with data downsampled to 32 frequency channels.

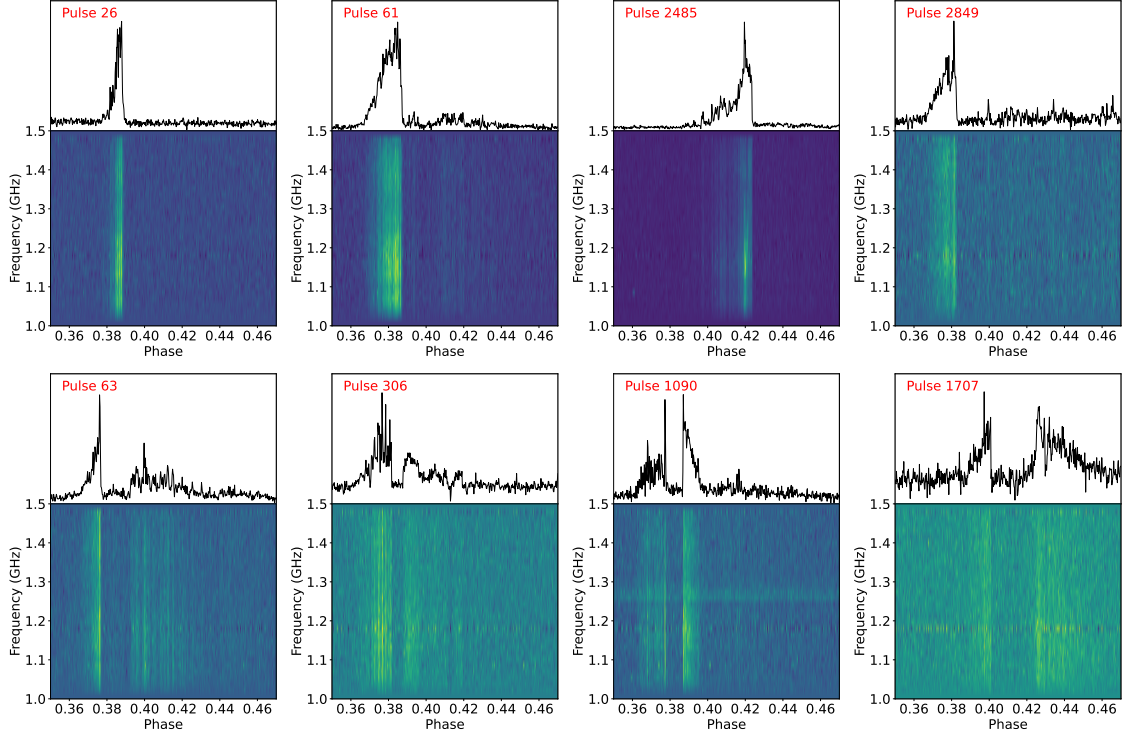


Figure 19. Gallery of partially nulling pulses and pulses exhibiting rapid intensity decay in the IP of PSR J0953+0755. Each panel features a pulse profile (top) and a phase-frequency intensity map (bottom), with data downsampled to 32 frequency channels.

energy from the width of the micropulses (Lange et al. 1998):

$$\gamma = \frac{P}{2\pi\tau_\mu \cdot \sin(\zeta)} \quad (1)$$

where γ is the Lorentz factor of the particles, P is the rotation period of pulsar, τ_μ is the characteristic timescale of microstructure, and $\zeta = \alpha + \beta$ is the angle between the line of sight and the rotation axis. Some researchers have argued that γ should not significantly exceed a value of 100 (Asseo 1993). However, derived γ values (from 240 to 520 (Lange et al. 1998)) often exceed theoretical expectations ($\gamma \leq 100$) from simpler curvature radiation models (Daugherty & Harding 1982). We also calculated the Lorentz factor for some pulsars. As shown in Table 6, all these γ are greater than 100. This significant discrepancy may suggest that such a model may not adequately account for the observed microstructure or the pulsar’s radiation may not conform to simple coherent curvature radiation models. Assuming that the γ is low, the next interpretation for the microstructure width is more likely to hold.

Temporal Modulation: Alternative models attribute microstructure to temporal or radial modulations within the magnetosphere. Temporal modulation via nonlinear plasma instabilities, such as two-stream instability, generates coherent radiation from charged solitons that excite extraordinary (X) and ordinary (O) modes in electron-positron plasmas (Melikidze et al. 2000). The absence of circular polarization sign reversals in observations supports this scenario, as plasma propagation effects disrupt phase coherence between modes, unlike vacuum curvature radiation from single particles (Mitra et al. 2015). Radial modulation models link microstructure duration to the thickness of emitting structures (e.g. plasma clouds), with radial lengths on the order of $c \cdot P_\mu$ (hundreds of kilometers for nanosecond pulses, as in the Crab pulsar; Hankins et al. (2003)). Interestingly, Thompson (2022a,b) link the radio emission of rotating neutron stars with slow tearing instabilities caused by uneven twisting in the open pulsar circuit. In this theory, radio emission comes from coherent curvature radiation generated by Cherenkov-like instabilities in current-carrying Alfvén waves within thin sheets of relativistic particle flow (Thompson 2022b). The model also predicts that directed radio radiation arises from clusters of charged particles, with quasi-periodic microstructure emerging naturally from these physical processes. The observed timescale of the microstructure, influenced by relativistic beaming, leads

to the derived relation $\tau_\mu \approx 1/(\Omega\gamma_{eff})$, which matches the observed relationship $P_\mu \approx 10^{-3}P$ (Thompson 2022b). This result suggests that all radio-emitting neutron stars might share the same effective Lorentz factor: $\gamma_{eff} \approx 200$. It is worth noting that the physical conditions associated with slow tearing instability are more significantly influenced by the local magnetic field strength. Additionally, the magnetic field of pulsars may not be a simple dipole field, which seemingly explains why there is no obvious correlation between the microstructure and the pulsar surface magnetic field derived under the dipole field assumption in M15.

Observational Constraints and Open Questions: Key evidence favoring magnetospheric origins includes the consistency of Stokes parameter periodicities (I, V, L), ruling out single-particle radiation (Mitra et al. 2015), and frequency-dependent width scaling consistent with radius-frequency mapping (Cordes 1976). However, unresolved issues persist: the discrepancy between beaming-model γ factors and theoretical limits and the role of polar cap asymmetry in generating component-specific microstructure (e.g. in PSR B1133+16; Popov et al. (2002)). It is worth noting that previous studies reported differences in the microstructure of different components (Popov et al. 2002), but the results presented in M15 indicate that there are no significant differences in the microstructure among different components. In this work, our results indicate that the τ_μ and P_μ of microstructure across components appear consistent within measurement errors for PSR J0627+0706, but microstructure in IP are relatively smaller than those in MP for PSR J0953+0755. Whether the microstructure of different components are consistent and what factors influence such differences require more observational evidence for further research. More importantly, how can we determine whether microstructures result from a combination of temporal modulation and angular beam models? Or, what level of time resolution is required in observations to conclude that the observed microstructures are dominated by temporal modulation? These questions still require further investigation.

In summary, while angular beaming and plasma modulation models provide complementary frameworks, integrating high-resolution polarization and multi-frequency data, especially for millisecond pulsars and magnetars, will be pivotal to resolving the interplay between particle acceleration, radiation geometry, and propagation effects in shaping pulsar microstructure.

5.2. Microstructure as a Probe for Correlations Between MP and IP

Based on the theoretical hypothesis that microstructures are formed by temporal modulation within magnetic flux tubes, and considering the relative stability of the time scales and characteristic periods of microstructures within the same magnetic flux tube, we can determine whether the interpulse (IP) and main pulse (MP) of pulsars originate from the same magnetic flux tube by comparing the similarities and differences of their microstructure. Generally, if the pulse signals originate from the same magnetic flux tube, their polarization properties maybe similar. In contrast, signals from different magnetic regions exhibit abrupt jumps in polarization phase and do not follow the S-shaped wings. Sun et al. (2025) conducted an in-depth study on the MP and IP of pulsars. Their results show that the observational data of PSR J0953+0755 conform to the characteristics of the Rotating Vector Model (RVM), suggesting that its MP and IP may originate from the same magnetic pole. Meanwhile, this pulsar shows a significant jump in the polarization position angle. A further detailed comparative analysis of the microstructures of the MP and IP of this pulsar reveals that the microstructures in the IP are more refined in size compared to those in the MP. Combining with the above-mentioned theoretical framework, this correlation in microstructure size provides strong observational evidence that the MP and IP of J0953+0755 originate from different magnetic flux tubes of the same magnetic pole. For PSR J0627+0706, its polarization properties deviate from the predictions of the RVM model, the polarization position angle of both MP and IP component exhibit abrupt jumps (Sun et al. 2025), the separation between the MP and IP components is approximately half a rotation period, and the microstructure in this pulsar show no significant differences between MP and IP. Thus, we conclude that the MP and IP components originate from two distinct magnetic poles, and the MP might share the same magnetic flux tube with part of the IP component. The pulse profile of PSR J0826+2637 is intriguing, composed of a MP, a subsequent post-cursor (PC), and an IP. Results from Sun et al. (2025) show that the polarization position angle of this pulsar exhibits a distinct jump in the phase between the MP and PC, and the phase separation between the MP and IP is approximately half a rotation period. Thus, we propose that the MP and IP originate from different magnetic poles and might share the same magnetic flux tube (we emphasize that this is not a robust conclusion due to the lack of comparative analysis in microstructure). Some studies suggest that pulsars may not strictly follow simple dipolar fields (Arumugasamy & Mitra 2019). Therefore, a plausible explanation is that the PC component originates from local strong magnetic field regions other than the dipolar field.

6. CONCLUSION

In this paper, we studied microstructure in four interpulse pulsars (PSRs J0953+0755 (B0950+08), J0627+0706, J0826+2637 (B0823+26) and J1946+1805 (B1944+17)) with FAST. The main conclusions are as follows:

1. For the first time, we detected the quasi-periodic microstructure in the interpulse of pulsars.
2. We found that microstructure, even quasi-periodic microstructure, seems to exist in the mainpulse and interpulse of all pulsars, except for interpulse of PSRs J0826+2637 and J1946+1805, and obtained the statistical results of characteristic timescales and characteristic periods of these microstructure.
3. The microstructure in mainpulse and interpulse were compared, and our results show that, for PSR J0627+0706, the characteristic timescales and characteristic periods of quasi-periodic microstructure between MP and IP are generally consistent within error ranges. However, for PSR J0953+0755, microstructure in IP may be smaller than those in MP.
4. The relationship between the characteristic period of microstructure and the rotation period in neutron star populations was reconfirmed: $P_{\mu}(\text{ms}) = (1.337 \pm 0.114) \times P(\text{s})^{(1.063 \pm 0.038)}$.

7. ACKNOWLEDGMENTS

This work was supported by the Major Science and Technology Program of Xinjiang Uygur Autonomous Region (No.2022A03013-4), the Guizhou Provincial Basic Research Program (Natural Science) (No. Qiankehejichu-MS(2025)263), the Guizhou Provincial Science and Technology Projects (Nos. QKHFQ[2023]003, QKHPTRC-ZDSYS[2023]003, QKHFQ[2024]001-1), Guizhou Provincial Scientific and Technological Program—the Postdoctoral Research Station of the Guizhou Radio Astronomical Observatory (No.QKHPTRC[2021] Postdoctoral Research Station-001), the National Natural Science Foundation of China (No. 12041304), the Project funded by China Postdoctoral Science Foundation(No. 2023M743517) and the Natural Science Basic Research Program of Shaanxi (Program No. 2024JC-YBQN-0036). This work made use of the data from FAST (Five-hundred-meter Aperture Spherical radio Telescope). FAST is a Chinese national mega-science facility, operated by National Astronomical Observatories, Chinese Academy of Sciences.

Software: PSRCHIVE (Hotan et al. 2004), DSPSR (van Straten & Bailes 2011), PSRCAT (Manchester et al. 2005) NumPy⁵ (Harris et al. 2020), Matplotlib⁶ (Hunter 2007) and SciPy⁷ (Virtanen et al. 2020).

REFERENCES

- Arumugasamy, P., & Mitra, D. 2019, MNRAS, 489, 4589, doi: [10.1093/mnras/stz2299](https://doi.org/10.1093/mnras/stz2299)
- Asseo, E. 1993, MNRAS, 264, 940, doi: [10.1093/mnras/264.4.940](https://doi.org/10.1093/mnras/264.4.940)
- Backer, D. C., Boriakoff, V., & Manchester, R. N. 1973, Nature Physical Science, 243, 77, doi: [10.1038/physci243077a0](https://doi.org/10.1038/physci243077a0)
- Bartel, N., Sieber, W., & Graham, D. A. 1980, A&A, 87, 282
- Basu, R., & Mitra, D. 2019, MNRAS, 487, 4536, doi: [10.1093/mnras/stz1590](https://doi.org/10.1093/mnras/stz1590)
- Beloborodov, A. M. 2017, ApJL, 843, L26, doi: [10.3847/2041-8213/aa78f3](https://doi.org/10.3847/2041-8213/aa78f3)
- Benford, G. 1977, MNRAS, 179, 311, doi: [10.1093/mnras/179.3.311](https://doi.org/10.1093/mnras/179.3.311)
- Bochenek, C. D., Ravi, V., Belov, K. V., et al. 2020, Nature, 587, 59, doi: [10.1038/s41586-020-2872-x](https://doi.org/10.1038/s41586-020-2872-x)
- Boriakoff, V. 1976, ApJL, 208, L43, doi: [10.1086/182229](https://doi.org/10.1086/182229)
- Boriakoff, V., & Ferguson, D. C. 1981, in Pulsars: 13 Years of Research on Neutron Stars, ed. W. Sieber & R. Wielebinski, Vol. 95, 191–196
- Caleb, M., Heywood, I., Rajwade, K., et al. 2022a, Nature Astronomy, 6, 828, doi: [10.1038/s41550-022-01688-x](https://doi.org/10.1038/s41550-022-01688-x)
- Caleb, M., Rajwade, K., Desvignes, G., et al. 2022b, MNRAS, 510, 1996, doi: [10.1093/mnras/stab3223](https://doi.org/10.1093/mnras/stab3223)
- Chen, J. L., Wen, Z. G., Yuan, J. P., et al. 2022, ApJ, 934, 24, doi: [10.3847/1538-4357/ac75d1](https://doi.org/10.3847/1538-4357/ac75d1)

⁵ <https://numpy.org/>

⁶ <https://matplotlib.org/>

⁷ <https://scipy.org/>

- Chen, J. L., Wen, Z. G., Duan, X. F., et al. 2023, *ApJ*, 946, 2, doi: [10.3847/1538-4357/acbd97](https://doi.org/10.3847/1538-4357/acbd97)
- CHIME/FRB Collaboration, Andersen, B. C., Bandura, K. M., et al. 2020, *Nature*, 587, 54, doi: [10.1038/s41586-020-2863-y](https://doi.org/10.1038/s41586-020-2863-y)
- Chime/Frb Collaboration, Andersen, B. C., Bandura, K., Bhardwaj, M., et al. 2022, *Nature*, 607, 256, doi: [10.1038/s41586-022-04841-8](https://doi.org/10.1038/s41586-022-04841-8)
- Cordes, J. M. 1976, *ApJ*, 208, 944, doi: [10.1086/154683](https://doi.org/10.1086/154683)
- Cordes, J. M., & Hankins, T. H. 1977, *ApJ*, 218, 484, doi: [10.1086/155702](https://doi.org/10.1086/155702)
- Cordes, J. M., Weisberg, J. M., & Hankins, T. H. 1990, *AJ*, 100, 1882, doi: [10.1086/115644](https://doi.org/10.1086/115644)
- Craft, H. D., Comella, J. M., & Drake, F. D. 1968a, *Nature*, 218, 1122, doi: [10.1038/2181122a0](https://doi.org/10.1038/2181122a0)
- Craft, H. D., Sutton, J. M., & Comella, J. M. 1968b, *Nature*, 219, 1237, doi: [10.1038/2191237a0](https://doi.org/10.1038/2191237a0)
- Dang, S. J., Yuan, J. P., Shang, L. H., et al. 2024, *MNRAS*, 528, 1213, doi: [10.1093/mnras/stae046](https://doi.org/10.1093/mnras/stae046)
- Daugherty, J. K., & Harding, A. K. 1982, *ApJ*, 252, 337, doi: [10.1086/159561](https://doi.org/10.1086/159561)
- De, K., Gupta, Y., & Sharma, P. 2016, *ApJL*, 833, L10, doi: [10.3847/2041-8213/833/1/L10](https://doi.org/10.3847/2041-8213/833/1/L10)
- Deich, W. T. S., Cordes, J. M., Hankins, T. H., & Rankin, J. M. 1986, *ApJ*, 300, 540, doi: [10.1086/163831](https://doi.org/10.1086/163831)
- Ferguson, D. C., Graham, D. A., Jones, B. B., Seiradakis, J. H., & Wielebinski, R. 1976, *Nature*, 260, 25, doi: [10.1038/260025a0](https://doi.org/10.1038/260025a0)
- Fiore, W., McLaughlin, M. A., Agazie, G., et al. 2024, *arXiv e-prints*, arXiv:2412.05452, doi: [10.48550/arXiv.2412.05452](https://doi.org/10.48550/arXiv.2412.05452)
- Hankins, T. H. 1971a, PhD thesis, University of California, San Diego
- . 1971b, *ApJ*, 169, 487, doi: [10.1086/151164](https://doi.org/10.1086/151164)
- Hankins, T. H., & Boriakoff, V. 1978, *Nature*, 276, 45, doi: [10.1038/276045a0](https://doi.org/10.1038/276045a0)
- Hankins, T. H., & Cordes, J. M. 1981, *ApJ*, 249, 241, doi: [10.1086/159281](https://doi.org/10.1086/159281)
- Hankins, T. H., & Fowler, L. A. 1986, *ApJ*, 304, 256, doi: [10.1086/164159](https://doi.org/10.1086/164159)
- Hankins, T. H., Kern, J. S., Weatherall, J. C., & Eilek, J. A. 2003, *Nature*, 422, 141, doi: [10.1038/nature01477](https://doi.org/10.1038/nature01477)
- Harris, C. R., Millman, K. J., van der Walt, S. J., et al. 2020, *Nature*, 585, 357, doi: [10.1038/s41586-020-2649-2](https://doi.org/10.1038/s41586-020-2649-2)
- Hermesen, W., Kuiper, L., Basu, R., et al. 2018, *MNRAS*, 480, 3655, doi: [10.1093/mnras/sty2075](https://doi.org/10.1093/mnras/sty2075)
- Hobbs, G., Lyne, A. G., Kramer, M., Martin, C. E., & Jordan, C. 2004, *MNRAS*, 353, 1311, doi: [10.1111/j.1365-2966.2004.08157.x](https://doi.org/10.1111/j.1365-2966.2004.08157.x)
- Hotan, A. W., van Straten, W., & Manchester, R. N. 2004, *PASA*, 21, 302, doi: [10.1071/AS04022](https://doi.org/10.1071/AS04022)
- Hunter, J. D. 2007, *Computing in Science & Engineering*, 9, 90, doi: [10.1109/MCSE.2007.55](https://doi.org/10.1109/MCSE.2007.55)
- Jenet, F. A., Anderson, S. B., Kaspi, V. M., Prince, T. A., & Unwin, S. C. 1998, *ApJ*, 498, 365, doi: [10.1086/305529](https://doi.org/10.1086/305529)
- Jessner, A., Popov, M. V., Kondratiev, V. I., et al. 2010, *A&A*, 524, A60, doi: [10.1051/0004-6361/201014806](https://doi.org/10.1051/0004-6361/201014806)
- Johnston, S., van Straten, W., Kramer, M., & Bailes, M. 2001, *ApJL*, 549, L101, doi: [10.1086/319154](https://doi.org/10.1086/319154)
- Keith, M. J., Johnston, S., Weltevrede, P., & Kramer, M. 2010, *MNRAS*, 402, 745, doi: [10.1111/j.1365-2966.2009.15926.x](https://doi.org/10.1111/j.1365-2966.2009.15926.x)
- Kloumann, I. M., & Rankin, J. M. 2010, *MNRAS*, 408, 40, doi: [10.1111/j.1365-2966.2010.17114.x](https://doi.org/10.1111/j.1365-2966.2010.17114.x)
- Kramer, M., Johnston, S., & van Straten, W. 2002, *MNRAS*, 334, 523, doi: [10.1046/j.1365-8711.2002.05478.x](https://doi.org/10.1046/j.1365-8711.2002.05478.x)
- Kramer, M., Liu, K., Desvignes, G., Karuppusamy, R., & Stappers, B. W. 2024, *Nature Astronomy*, 8, 230, doi: [10.1038/s41550-023-02125-3](https://doi.org/10.1038/s41550-023-02125-3)
- Kuzmin, A. D., Hamilton, P. A., Shitov, Y. P., et al. 2003, *MNRAS*, 344, 1187, doi: [10.1046/j.1365-8711.2003.06900.x](https://doi.org/10.1046/j.1365-8711.2003.06900.x)
- Lange, C., Kramer, M., Wielebinski, R., & Jessner, A. 1998, *A&A*, 332, 111
- Lee, Y. W. J., Caleb, M., Murphy, T., et al. 2025, *Nature Astronomy*, 9, 393, doi: [10.1038/s41550-024-02452-z](https://doi.org/10.1038/s41550-024-02452-z)
- Liu, K., Bassa, C. G., Janssen, G. H., et al. 2016, *MNRAS*, 463, 3239, doi: [10.1093/mnras/stw2223](https://doi.org/10.1093/mnras/stw2223)
- Liu, K., Antoniadis, J., Bassa, C. G., et al. 2022, *MNRAS*, 513, 4037, doi: [10.1093/mnras/stac1082](https://doi.org/10.1093/mnras/stac1082)
- Lower, M. E., Bailes, M., Shannon, R. M., et al. 2020, *MNRAS*, 494, 228, doi: [10.1093/mnras/staa615](https://doi.org/10.1093/mnras/staa615)
- Lyubarsky, Y. 2014, *MNRAS*, 442, L9, doi: [10.1093/mnrasl/slu046](https://doi.org/10.1093/mnrasl/slu046)
- Maciesiak, K., Gil, J., & Ribeiro, V. A. R. M. 2011, *MNRAS*, 414, 1314, doi: [10.1111/j.1365-2966.2011.18471.x](https://doi.org/10.1111/j.1365-2966.2011.18471.x)
- Majid, W. A., Pearlman, A. B., Prince, T. A., et al. 2021, *ApJL*, 919, L6, doi: [10.3847/2041-8213/ac1921](https://doi.org/10.3847/2041-8213/ac1921)
- Manchester, R. N., Hobbs, G. B., Teoh, A., & Hobbs, M. 2005, *AJ*, 129, 1993, doi: [10.1086/428488](https://doi.org/10.1086/428488)
- Manchester, R. N., & Lyne, A. G. 1977, *MNRAS*, 181, 761, doi: [10.1093/mnras/181.4.761](https://doi.org/10.1093/mnras/181.4.761)
- Melikidze, G. I., Gil, J. A., & Pataraya, A. D. 2000, *ApJ*, 544, 1081, doi: [10.1086/317220](https://doi.org/10.1086/317220)
- Mitra, D., Arjunwadkar, M., & Rankin, J. M. 2015, *ApJ*, 806, 236, doi: [10.1088/0004-637X/806/2/236](https://doi.org/10.1088/0004-637X/806/2/236)
- Mitra, D., Basu, R., Melikidze, G. I., & Arjunwadkar, M. 2020, *MNRAS*, 492, 2468, doi: [10.1093/mnras/stz3620](https://doi.org/10.1093/mnras/stz3620)

- Niu, J.-R., Zhu, W.-W., Zhang, B., et al. 2022, *Research in Astronomy and Astrophysics*, 22, 124004, doi: [10.1088/1674-4527/ac995d](https://doi.org/10.1088/1674-4527/ac995d)
- Pastor-Marazuela, I., van Leeuwen, J., Bilous, A., et al. 2023, *A&A*, 678, A149, doi: [10.1051/0004-6361/202243339](https://doi.org/10.1051/0004-6361/202243339)
- Pilkington, J. D. H., Hewish, A., Bell, S. J., & Cole, T. W. 1968, *Nature*, 218, 126, doi: [10.1038/218126a0](https://doi.org/10.1038/218126a0)
- Popov, M. V., Bartel, N., Cannon, W. H., et al. 2002, *A&A*, 396, 171, doi: [10.1051/0004-6361:20021402](https://doi.org/10.1051/0004-6361:20021402)
- Sobey, C., Young, N. J., Hessels, J. W. T., et al. 2015, *MNRAS*, 451, 2493, doi: [10.1093/mnras/stv1066](https://doi.org/10.1093/mnras/stv1066)
- Soglasnov, V. A., Smirnova, T. V., Popov, M. V., & Kuz'min, A. D. 1981, *Soviet Ast.*, 25, 442
- Sun, S. N., Wang, N., Yan, W. M., & Wang, S. Q. 2025, *arXiv e-prints*, arXiv:2503.13824, doi: [10.48550/arXiv.2503.13824](https://doi.org/10.48550/arXiv.2503.13824)
- Tang, Z., Zhang, S., Wang, J., Yang, X., & Wu, X. 2025, *MNRAS*, doi: [10.1093/mnras/staf570](https://doi.org/10.1093/mnras/staf570)
- Thompson, C. 2022a, *ApJ*, 933, 231, doi: [10.3847/1538-4357/ac501f](https://doi.org/10.3847/1538-4357/ac501f)
- . 2022b, *ApJ*, 933, 232, doi: [10.3847/1538-4357/ac51d4](https://doi.org/10.3847/1538-4357/ac51d4)
- Tian, J., Xu, X., Bai, J., et al. 2024, *Ap&SS*, 369, 21, doi: [10.1007/s10509-024-04284-9](https://doi.org/10.1007/s10509-024-04284-9)
- van Straten, W., & Bailes, M. 2011, *PASA*, 28, 1, doi: [10.1071/AS10021](https://doi.org/10.1071/AS10021)
- Vaughan, A. E., & Large, M. I. 1970, *Nature*, 225, 167, doi: [10.1038/225167a0](https://doi.org/10.1038/225167a0)
- Virtanen, P., Gommers, R., Oliphant, T. E., et al. 2020, *Nature Methods*, 17, 261, doi: [10.1038/s41592-019-0686-2](https://doi.org/10.1038/s41592-019-0686-2)
- Wang, N., Manchester, R. N., & Johnston, S. 2007, *MNRAS*, 377, 1383, doi: [10.1111/j.1365-2966.2007.11703.x](https://doi.org/10.1111/j.1365-2966.2007.11703.x)
- Wang, Z., Lu, J., Jiang, J., et al. 2022, *MNRAS*, 517, 5560, doi: [10.1093/mnras/stac3026](https://doi.org/10.1093/mnras/stac3026)
- Yang, H., Dang, S., Zhi, Q., et al. 2023, *Universe*, 9, 50, doi: [10.3390/universe9010050](https://doi.org/10.3390/universe9010050)
- Zhang, S. B., Geng, J. J., Wang, J. S., et al. 2024, *ApJ*, 972, 59, doi: [10.3847/1538-4357/ad6602](https://doi.org/10.3847/1538-4357/ad6602)
- Zhong, W., Zhi, Q., Lu, J., et al. 2024, *MNRAS*, 527, 4129, doi: [10.1093/mnras/stad3402](https://doi.org/10.1093/mnras/stad3402)